ELSEVIER

Journal of Alloys and Compounds 303–304 (2000) 1–29

Journal of ALLOYS AND COMPOUNDS

www.elsevier.com/locate/jallcom

# Three decades of prospecting for novel electronic states and phenomena in f-electron materials

M. Brian Maple*

*Department of Physics and Institute for Pure and Applied Physical Sciences, University of California, 9500 Gilman Drive, La Jolla, San Diego, CA 92093-0319, USA*

**Abstract**

During the past three decades, f-electron materials have proven to be a rich reservoir of novel electronic states and extraordinary superconducting and magnetic phenomena, many of which are surveyed in this paper. The electronic states described include the non-magnetic Kondo many-body singlet, valence fluctuation, heavy fermion, and non-Fermi liquid states. The superconducting and magnetic phenomena recounted include reentrant superconductivity due to the Kondo effect or the onset of ferromagnetic order, the sinusoidally modulated magnetic state that coexists with superconductivity in ferromagnetic superconductors, coexistence of superconductivity and antiferromagnetic order, pressure-induced demagnetization of rare earth ions in dilute and concentrated rare earth systems, and anisotropic superconductivity in which the energy gap vanishes at points or on lines on the Fermi surface, possibly mediated by spin fluctuations, in heavy fermion f-electron and high-$T_c$ cuprate superconductors. The temperature vs. pressure or composition phase diagrams of f-electron compounds and high-$T_c$ cuprate superconductors in the vicinity of their antiferromagnetic quantum critical points are briefly compared. 

*Keywords:* Rare earth; Actinide; Superconductivity; Magnetism; Valence fluctuations; Kondo effect; Heavy fermion; Non-Fermi liquid

## 1. Introduction

It is a great honor to have been selected for the 9th Frank H. Spedding Award for research on the rare earths. This award is a real tribute to a long list of talented individuals with whom I have been privileged to work on the physics of f-electron materials throughout my career. Included in this list are many bright young graduate students and postdoctoral researchers who have passed through our laboratory at UCSD, as well as numerous colleagues and collaborators at UCSD and other institutions throughout the world.

The title of this paper, 'Three decades of prospecting for novel electronic states and phenomena in f-electron materials,' reflects several aspects of my relationship with rare earth and actinide materials throughout my research career: My fascination with f-electron materials has spanned more than three decades, an integral part of my research activities over the years can be described as a type of 'prospecting,' and f-electron materials have proven to be a literal 'gold mine' of new electronic states and extraordinary superconducting and magnetic phenomena. I think it is fair to say that the wealth of spectacular and largely unexpected discoveries that have emerged from the worldwide research effort on f-electron materials during the past three decades has exceeded our wildest expectations. It has indeed been rewarding to have participated in this exciting enterprise. Some of the electronic states and superconducting and magnetic phenomena that have been discovered are listed below in Section 2.

I first became involved in research on rare earth materials in 1967 when I was a graduate student at UCSD working in the laboratory of Prof. Bernd T. Matthias. At that time, the behavior of rare earth ions in metals was thought to be well understood. Because the hybridization of localized 4f and conduction electron states for most rare earth ions is weak and the electronic correlations within the 4f shell are strong, rare earth (R) ions in metals were generally found to display the same ionic local magnetic behavior as they did in insulators: (i) the magnetic susceptibility usually conforms to a Curie–Weiss law at high temperatures; (ii) the magnetic susceptibility of Sm and Eu ions exhibit Van Vleck anomalies due to the small multiplet splittings of these ions; and (iii) the magnetic susceptibility and specific heat display features (Schottky

*Fax: +1-585-534-1241.

*E-mail address:* mbmaple@ucsd.edu (M.B. Maple)

0925-8388/00/$ – see front matter 
PII: S0925-8388(00)00596-X

anomalies in the case of the specific heat) that are associated with crystalline electric field (CEF) splitting of the R ion's Hunds' rule multiplet. As a result, metallic rare earth systems were regarded as rather uninteresting, especially with respect to the formation of localized magnetic moments in metals. At the time, magnetic moment formation in metals was a major unsolved problem in condensed matter physics in which transition metals held center stage. After learning about the experiments Dieter Wohlleben and I had been performing in the early 1970s on magnetic moment formation of rare earth ions in metals, the late Peter Wohlfarth, coinventor of the famous Stoner–Wohlfarth model of itinerant ferromagnetism and a leading figure in the field of magnetism, exhorted: ''The rare earths are for boys; the transition metals are for men!'' While the judgement of our friend Peter Wohlfarth was usually right on the mark, I believe that research during the past three decades has demonstrated that his assessment of the rare earths was incorrect — in fact, the rare earths are for men, too!

This paper is based on the 9th Frank H. Spedding Award Lecture given by the author at the 22nd Rare Earth Research Conference in Argonne, IL. Some of the remarkable electronic states and superconducting and magnetic phenomena that have been discovered in f-electron materials during the past three decades were briefly surveyed in this lecture. The survey was made from a personal, historical perspective, drawing primarily upon examples from the author's research, and is recounted in the following.

## 2. Electronic states and superconducting and magnetic phenomena

Listed below are some of the more notable electronic states and superconducting and magnetic phenomena that have been discovered in f-electron materials during the past three decades. Most of these electronic states and phenomena are considered in this paper.

### *2.1. Electronic states*

Novel electronic states include: (i) an intermediate valence state in which a rare earth ion with a partially filled 4f-electron shell undergoes temporal fluctuations between two integral valence states that differ by one electron; (ii) a metallic heavy electron (or heavy fermion) state in which the conduction electrons have enormous effective masses as high as several hundred times the mass of the free electron; (iii) a low-temperature non-Fermi liquid state in which the physical properties have temperature and frequency dependences that violate the Fermi liquid paradigm; and (iv) an insulating phase with a small energy gap of several meV due to hybridization of localized f-electron and conduction electron states (these materials are referred to as hybridization gap semiconductors or Kondo insulators).

### *2.2. Superconducting and magnetic phenomena*

Extraordinary superconducting and magnetic phenomena include: (i) the destruction of superconductivity at a second critical temperature $T_{c2}<T_{c1}$, where $T_{c1}$ is the superconducting critical temperature (referred to as reentrant superconductivity) in a superconducting material containing paramagnetic impurities that exhibits the Kondo effect; (ii) the coexistence of superconductivity and antiferromagnetic order; (iii) the destruction of superconductivity by the onset of ferromagnetic order at a second critical temperature $T_{c2} \lesssim \theta_c < T_{c1}$, where $\theta_c$ is the Curie temperature and $T_{c1}$ is the superconducting critical temperature: (iv) the development of a new sinusoidally modulated magnetic state with a wavelength $\lambda \sim 10^2$ Å that coexists with superconductivity in a narrow temperature range above $T_{c2}$ due to superconducting–ferromagnetic interactions; (v) magnetic field-induced superconductivity (known as the Jaccarino–Peter effect); (vi) an unconventional superconducting state in which electrons are paired in singlet or triplet spin states with angular momentum greater than 0, possibly mediated by antiferromagnetic or ferromagnetic spin fluctuations (believed to occur in high-$T_c$ cuprate, heavy fermion, and organic superconductors); and (vii) multiple superconducting phases in heavy fermion superconductors.

## 3. Paramagnetic impurities in superconductors

My first encounter with rare earth materials was in the late 1960s when I embarked on studies of the effect of paramagnetic impurities on superconductivity. This work was motivated by the experiments of Matthias, Suhl and Corenzwit in 1958 [1] which revealed that the substitution of R ions with partially filled 4f electron shells into the superconducting element La, which has a superconducting critical temperature $T_c$ of ~6 K in its fcc phase, produces a rapid and nearly linear depression of $T_c$ with R impurity concentration $n$. Furthermore, it was found that the initial rate of depression of $T_c$ with $n$, $(-\mathrm{d}T_c/\mathrm{d}n)_{n=0}$, has a maximum in the middle of the R series at R=Gd, where the 4f electron shell is half-filled, and correlates with the spin $S$, rather than the effective moment, $\mu_{\mathrm{eff}}$, of the R ion. This lead Herring [2] and Suhl and Matthias [3] to suggest that the exchange interaction between the conduction electron spin $\boldsymbol{s}$ and the total angular momentum $\boldsymbol{J}=\boldsymbol{L}+\boldsymbol{S}$ of the R ion's Hund's rule multiplet is responsible for the depression of $T_c$. For R ions, the Hamiltonian $\mathcal{H}_{\mathrm{ex}}$ describing the exchange interaction has the form:

$$\mathcal{H}_{\mathrm{ex}} = -2(g_J-1)\mathcal{J}\boldsymbol{J}\cdot\boldsymbol{s} \quad (1)$$

where $g_J$ is the Landé $g$-factor of the R ion and $\mathcal{J}$ is the exchange interaction parameter. According to calculations based on this interaction within the framework of the pair breaking theory of Abrikosov and Gor'kov (AG) [4,5], the initial rate of depression of $T_c$, $(-dT_c/dn)_{n=0}$, should be proportional to $\mathcal{J}^2\mathcal{D}(R)$, where $\mathcal{D}(R) \equiv (g_J - 1)^2 J(J+1)$ is the deGennes factor [6]. The variation of $(-dT_c/dn)_{n=0}$ with R for the $La_{1-x}R_x$ system scales with the function $\mathcal{D}(R)$ if $\mathcal{J}^2$ is assumed to decrease slightly with increasing R atomic number, except for Ce where $(-dT_c/dn)_{n=0}$ is anomalously large [1]. Our investigations of the effect of substituted R ions on superconductivity of $LaAl_2$, which has a $T_c$ of 3.3 K, revealed a variation of $(-dT_c/dn)_{n=0}$ with R similar to that of $La_{1-x}R_x$, with a corresponding anomalously large rate of depression of $T_c$ with $n$ for R=Ce [7]. The $(-dT_c/dn)_{n=0}$ vs. R data for both $La_{1-x}R_x$ and $La_{1-x}R_xAl_2$, normalized to the value for Gd, are displayed in Fig. 1 [7,8].

The anomalous depression of $T_c$ with $n$ for Ce substituents in La and $LaAl_2$ is associated with the hybridization of the localized 4f electron states of Ce and the conduction electron states [8]. The hybridization generates a large negative contribution to the exchange interaction of the form:

$$\mathcal{J} \sim -\langle V_{kf}^2 \rangle / \varepsilon_f \quad (2)$$

where $V_{kf}$ is the matrix element which admixes Ce 4f and conduction electron states, $\varepsilon_f = E_F - E_f$ is the f-electron binding energy, $E_F$ is the Fermi energy, and $E_f$ is the energy of the centroid of the f state. The large depression of $T_c$ with Ce concentration is due to the large negative contribution to the exchange interaction and the occurrence of the Kondo effect with $T_K \sim T_{co}$, where $T_K$ is the Kondo temperature and $T_{co}$ is the $T_c$ of the La or $LaAl_2$ matrix (see below).

These experiments also yielded some stunning surprises. For example, we found that the curve of $T_c$ vs. Gd concentration $n$ for the $La_{1-x}Gd_xAl_2$ system could be well represented by the AG pair breaking theory [4,5] for superconductors containing paramagnetic impurities [9], providing the first confirmation of the AG theoretical calculation of the superconducting–normal phase boundary. Shown in Fig. 2 is a plot of $T_c/T_{co}$ vs. $n/n_{cr}$ for the $La_{1-x}Gd_xAl_2$ system; $T_{co}$ is the $T_c$ of the $LaAl_2$ host compound ($x=0$) and $n_{cr}$ is the critical concentration where $T_c$ vanishes. The solid line which has been fitted to the $T_c/T_{co}$ vs. $n/n_{cr}$ data is the AG theoretical curve. Also shown in Fig. 2 are the Curie–Weiss temperatures $\theta_p$, plotted as $\theta_p/T_{co}$ vs. $n/n_{cr}$, for the $La_{1-x}Gd_xAl_2$ system where the solid line is a guide to the eye [9,10]. Apparently, interactions between the Gd magnetic moments are sufficiently weak in this system to allow the AG theory to be tested to concentrations in the vicinity of $n_{cr}$.

Another surprise, which emerged from electrical resistivity measurements in the normal state of the $La_{1-x}Ce_xAl_2$ system, performed in collaboration with Zachary Fisk, was the occurrence of a Kondo effect, as evidenced by a minimum in $\rho(T)$ at low temperatures [11]. The Ce impurity contribution to $\rho(T)$ was found to diverge as $-\ln T$ with decreasing $T$ down to ~1 K, indicating a low Kondo temperature $T_K \lesssim 1$ K. The Kondo temperature

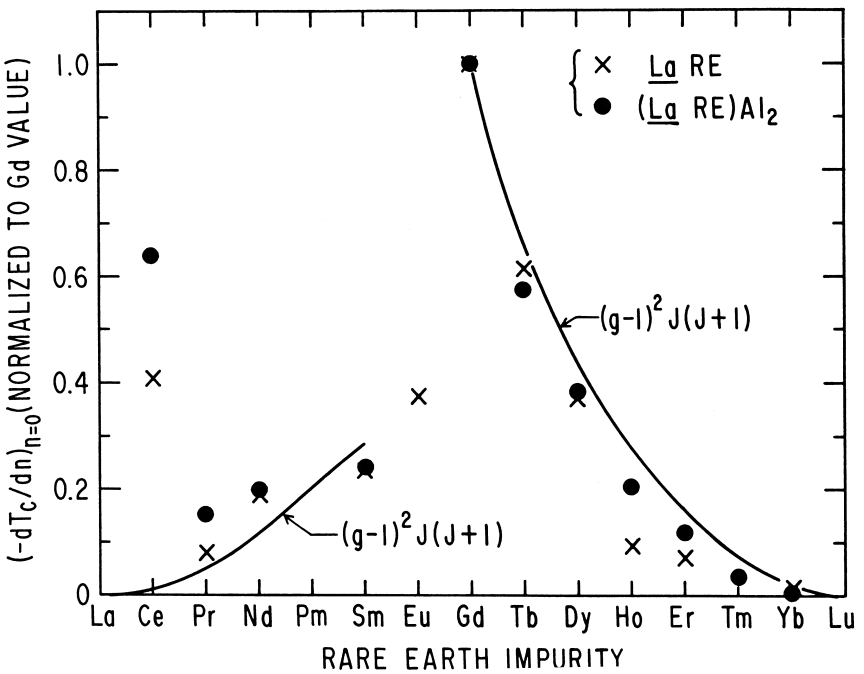


Fig. 1. Initial rate of depression of the superconducting critical temperature $T_c$ with paramagnetic impurity concentration $n$, $(-dT_c/dn)_{n=0}$, vs. rare earth R impurity for the $La_{1-x}R_x$ and $La_{1-x}R_xAl_2$ systems. After Refs. [7,8].

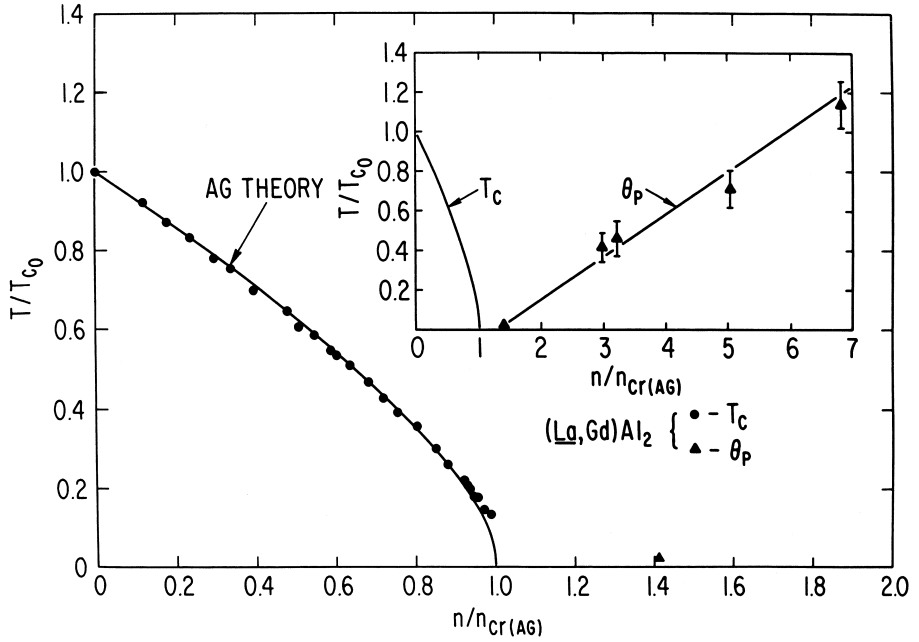


Fig. 2. Reduced superconducting critical temperature $T_c/T_{co}$ vs. reduced Gd impurity concentration $n/n_{cr}$ for the $La_{1-x}Gd_xAl_2$ system. The value of the superconducting critical temperature $T_{co}$ of the $LaAl_2$ host compound is 3.3 K, while the value of the critical concentration $n_{rc}$, where $T_c=0$, is 0.59 at.% Gd. The line denoted AG is the theoretical curve of Abrikosov and Gor'kov [4,5] that has been fitted to the data. Inset: Curie–Weiss temperatures $\theta_p$ determined from magnetic susceptibility measurements, plotted as $\theta_p/T_{co}$ vs. $n/n_{cr}$. The line through the data is a guide to the eye. After Refs. [9,10].

is a characteristic temperature that separates high-temperature magnetic behavior, where $\chi(T)$ behaves as a Curie–Weiss law, from low-temperature non-magnetic behavior, where $\chi(T)$ approaches a constant value. A physical picture of the non-magnetic groundstate that has emerged from theories of the Kondo effect involves the gradual formation as $T$ decreases through $T_K$ of a many-body singlet groundstate in which the spin of each paramagnetic impurity ion is screened by antiferromagnetically aligned spins of the conduction electrons. At the time, we felt somewhat uneasy about this result, since this was the first time a Kondo effect had been observed in a system in which the host was a compound, rather than an element. Of course, in retrospect, it now seems perfectly reasonable.

Further investigations of the $La_{1-x}Ce_xAl_2$ system revealed the phenomenon of reentrant superconductivity, wherein a sample within a certain range of Ce impurity concentrations becomes superconducting below a critical temperature $T_{c1}$ and then loses its superconductivity below a second critical temperature $T_{c2}$ [12,13]. The destruction of superconductivity at $T_{c2}$ is associated with the competition between singlet spin pairing of electrons in the superconducting state with characteristic energy $k_BT_c$ and the formation of the Kondo many-body singlet state involving the conduction electrons and each Ce impurity ion with characteristic energy $k_BT_K$. Shown in Fig. 3(a) and (b), respectively, are AC magnetic susceptibility vs. temperature data and the reentrant $T_c$ vs. $n$ curve of the $La_{1-x}Ce_xAl_2$ system. The values of $T_c$ in Fig. 3(b) and the transition curves in Fig. 3(a) from which they were inferred are identified with letters [13]. Subsequently, we discovered reentrant superconductivity in the $(La_{1-y}Th_y)_{1-x}Ce_x$ system in the low Th concentration range $0<y\leq0.25$ [14]. The Kondo anomalies in the normal state properties of the $La_{1-x}Ce_xAl_2$ system have also been well characterized and used to test theoretical models of the Kondo effect. Shown in Fig. 4 are specific heat $C$ vs. $T$ data for a $La_{1-x}Ce_xAl_2$ alloy ($x=0.064$) in various magnetic fields up to 38 kOe [15]. Curves (a)–(c), which have been drawn to fit more accurate data for a $La_{1-x}Ce_xAl_2$ alloy with $x=0.0906$, correspond to an entropy of $R$ ln(2) per mol Ce, showing that the $Ce^{3+}$ ground state is a doublet. Curve (d) is consistent with calculations of Bloomfield and Hamann [16] for $S=1/2$ and $T_K=0.42$ K. The two zero-field superconducting critical temperatures $T_{c1}$ and $T_{c2}$ are indicated by arrows in the figure.

Several experiments were conducted in collaboration with John Huber on superconducting matrix–impurity systems in which the impurity ion exhibited non-magnetic behavior at superconducting temperatures (i.e. $T_{co}\ll T_o$, where $T_o$ is a characteristic temperature that separates low-temperature non-magnetic behavior from high-temperature magnetic behavior, such as the Kondo temperature $T_K$). We found that the $T_c$ vs. $n$ curves have positive curvature and could be described by a modified exponential relation of the form:

$$T_c = T_{co}\exp[-An/(1-Dn)] \quad (3)$$

which had been proposed by Kaiser [17] who considered the effect of non-magnetic resonant d- and f-electron states

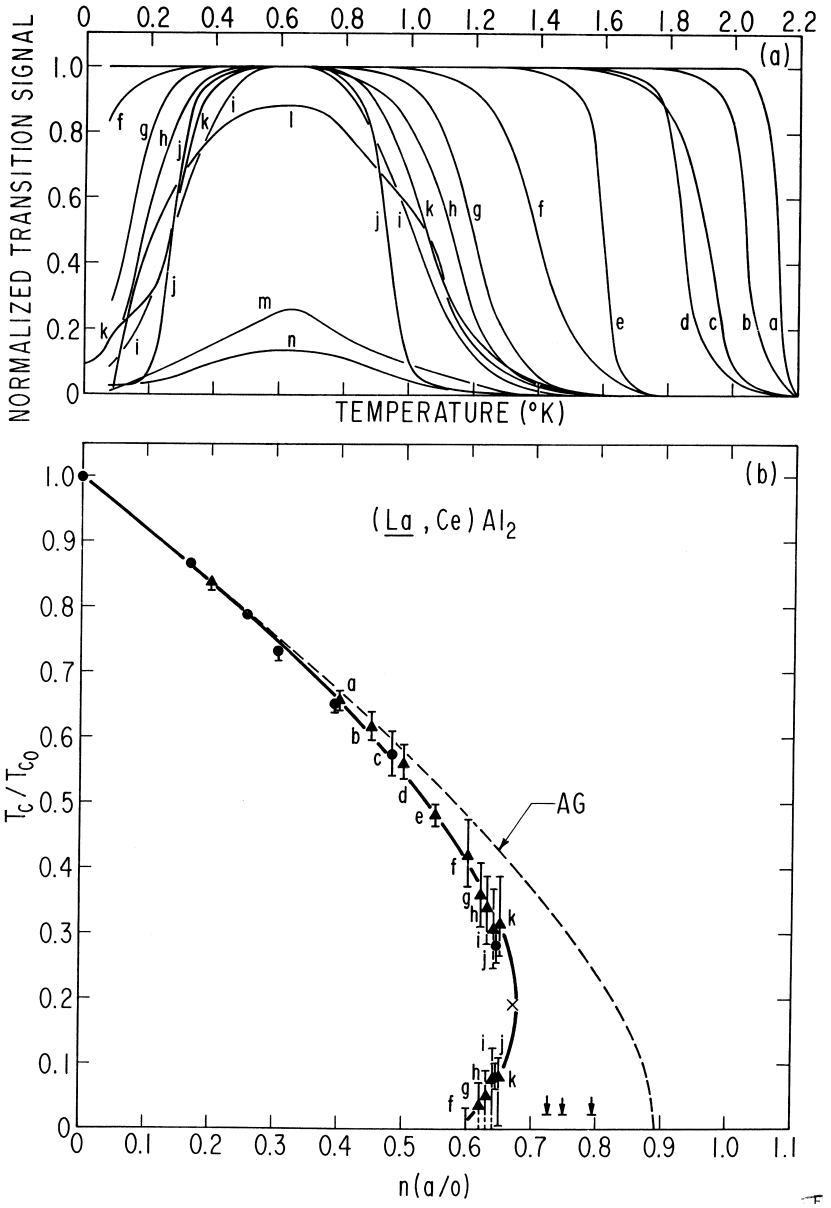


Fig. 3. (a) Normalized transition signal, based on AC magnetic susceptibility measurements, vs. temperature for the $La_{1-x}Ce_xAl_2$ system. (b) Reduced superconducting critical temperature $T_c/T_{co}$ vs. Ce impurity concentration $n$ for the $La_{1-x}Ce_xAl_2$ system. The value of the superconducting critical temperature $T_{co}$ of the $LaAl_2$ host compound is 3.3 K. The data identified by letters are derived from the corresponding transition curves in (a). After Ref. [13].

of impurity ions on superconductivity. Shown in Fig. 5 are plots of $T_c/T_{co}$ vs. $n/n_o$ for three systems [18] in which $T_o \gg T_{co}$, $Th_{1-x}U_x$ [19], $Th_{1-x}Ce_x$ [20], and $Al_{1-x}Mn_x$ [21]. An interesting example of the Kondo effect in the electrical resistivity is found in the $Th_{1-x}U_x$ system [19]. Shown in Fig. 6 are: (a) $\rho$ vs. $T$ data for $Th_{1-x}U_x$ samples with $x=0$, 0.01, 0.015 and 0.02, in which the resistivity minimum phenomenon is evident; and (b) $\Delta\rho$ vs. $T^2$ data, where $\Delta\rho(x,T) = \rho(x,T) - \rho(0,T)$ is the U contribution to the resistivity, that can be described by the relation $\Delta\rho(x,T) = \Delta\rho(x,0)[1 - (T/T_K)^2]$ with $T_K \approx 100$ K, consistent with the local Fermi liquid behavior expected for the Kondo effect at low temperatures $T \ll T_K$ [19].

Reentrant superconductivity associated with the Kondo effect was predicted to occur in the limit $T_K \ll T_{co}$, where $T_{co}$ is the critical temperature of the superconducting host metal, by Müller–Hartmann and Zittartz (MHZ) [22] and Ludwig and Zuckermann (LZ) [23]. MHZ and LZ obtained exponential-like curves of $T_c$ vs. $n$ in the limit $T_K \gg T_{co}$. Calculations of Zuckermann [24] and MHZ [24] for the initial depression of $T_c$ with $n$, $(-dT_c/dn)_{n=0}$, yielded a maximum as a function of $T_K/T_{co}$ at $T_K/T_{co} \approx 10$.

From our studies of the $La_{1-x}Ce_xAl_2$ system, we found that the resistivity minimum persisted to $x=1$ [26,27], suggesting that $CeAl_2$ exhibited a Kondo effect itself!

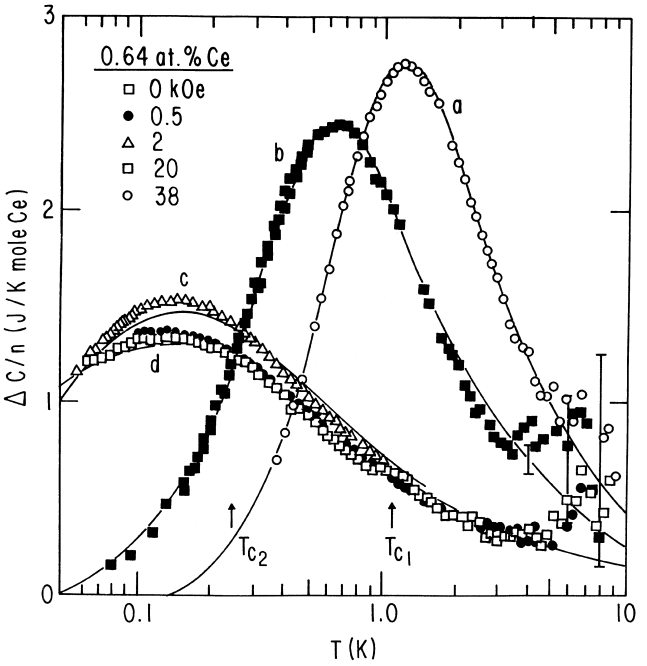


Fig. 4. Heat capacity $\Delta C/n$ of a $La_{1-x}Ce_xAl_2$ alloy ($x=0.064$) vs. temperature $T$ in various magnetic fields up to 38 kOe. Curves (a)–(c), which have been drawn to fit more accurate data for a $La_{1-x}Ce_xAl_2$ alloy with $x=0.0906$, correspond to an entropy of $R$ ln 2 per mol Ce, showing that the $Ce^{3+}$ ground state is a doublet. Curve (d) is consistent with calculations of Bloomfield and Hamann [16] for $S=1/2$ and $T_K=0.42$ K. The two zero-field superconducting critical temperatures are indicated. After Ref. [15].

Shown in Fig. 7 are plots of: (a) the inverse magnetic susceptibility $\chi^{-1}$ vs. temperature $T$ for $CeAl_2$; and (b) the electrical resistivity $\rho$ vs. $T$ curves for $CeAl_2$ and $LaAl_2$ [27]. The deviation in $\chi(T)$ from Curie–Weiss behavior below ~100 K is due to crystalline electric field (CEF) splitting of the $J=5/2$ Hund's rule multiplet into a $\Gamma_7$ doublet ground state and a $\Gamma_8$ quartet excited state with a splitting of ~100 K, while the cusp-like feature at 3.5 K is due to antiferromagnetic ordering. We attributed the rapid drop in $\rho(T)$ with decreasing $T$ to the thermal depopulation of the $\Gamma_8$ quartet excited state, the resistivity minimum followed by the increase of $\rho(T)$ with decreasing $T$ to the Kondo effect, and the sharp drop with decreasing $T$ at ~3.5 K to the decrease in the spin disorder resistivity associated with antiferromagnetic ordering. Before we were able to publish our findings, however, similar results were reported by van Daal and Buschow [28,29]. They were kind enough to acknowledge our work in a subsequent publication [30].

## 4. Pressure-induced demagnetization of rare earth ions

The application of high pressure turned out to be a particularly useful way of investigating novel phenomena in f-electron materials. One of my first assignments in 1963 as a young graduate student in the Matthias group was to design a high-pressure cell for studying supercon-

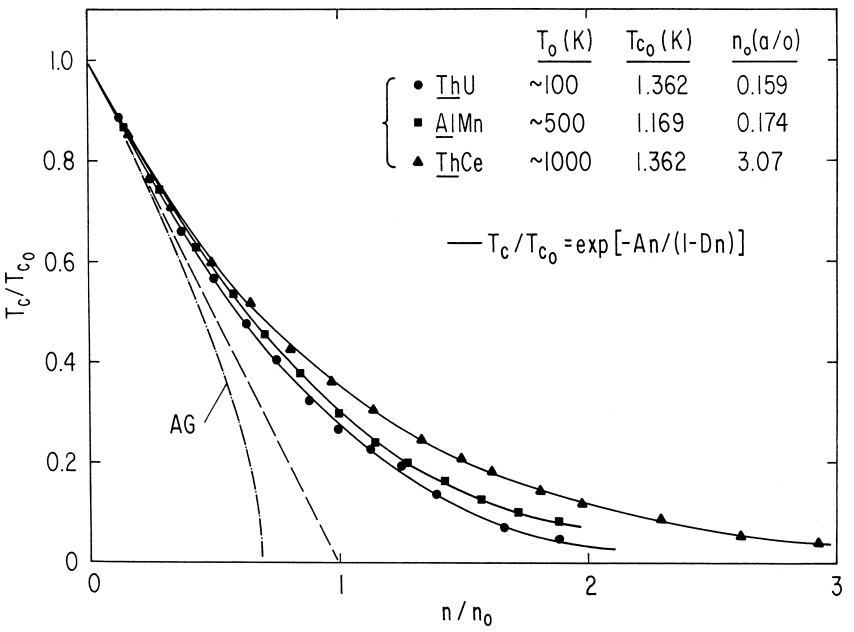


Fig. 5. Reduced superconducting critical temperature $T_c/T_{co}$ vs. reduced impurity concentration $n/n_o$ for the $Th_{1-x}Ce_x$, $Th_{1-x}U_x$, and $Al_{1-x}Mn_x$ systems. The solid lines represent the modified exponential relation given in the figure that describes the weakening of superconducting electron pairs by non-magnetic localized states [17]. The values of the characteristic (or Kondo) temperature $T_o$, superconducting critical temperature of the host $T_{co}$, and the scaling concentration $n_o$ are indicated in the figure. After Ref. [18].

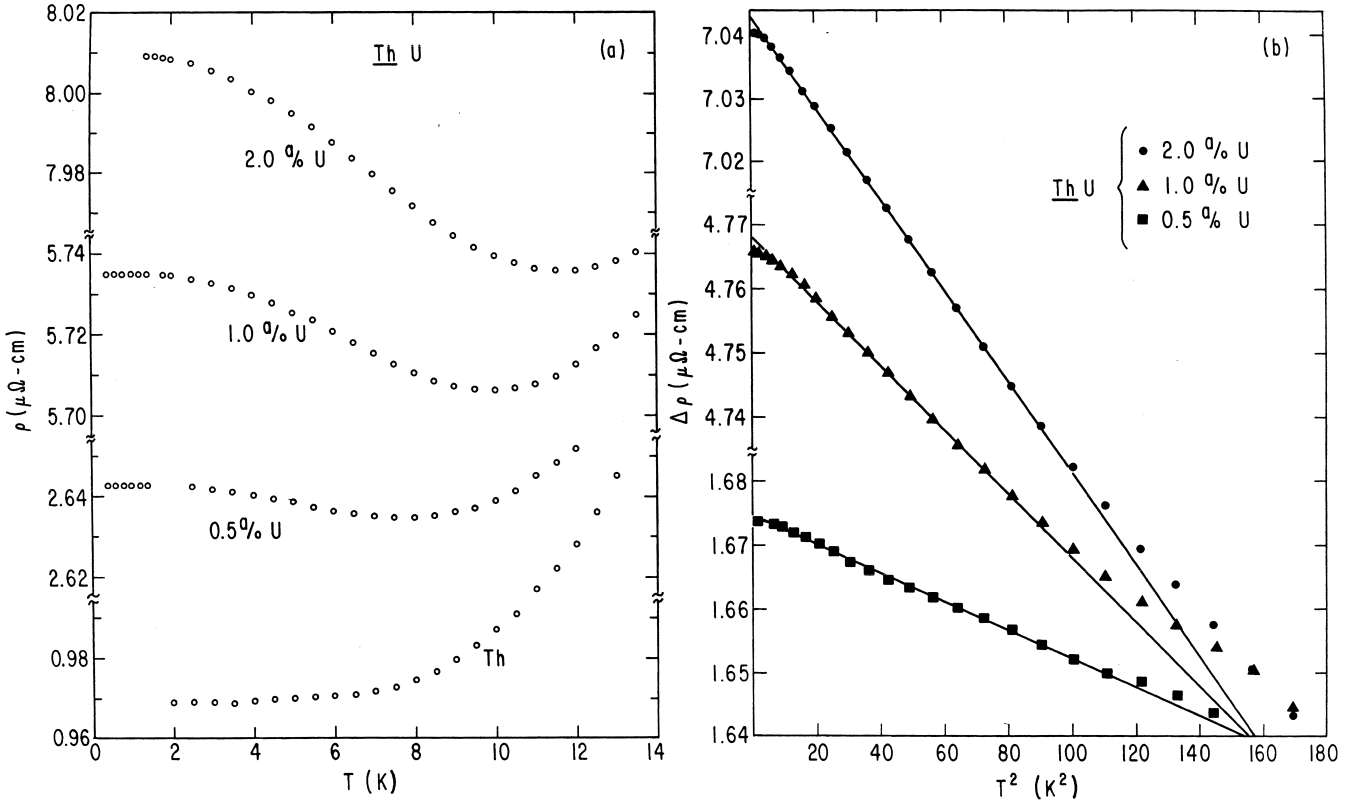


Fig. 6. (a) Electrical resistivity $\rho$ vs. temperature $T$ of $Th_{1-x}U_x$ alloys with $x=0$, 0.005, 0.01 and 0.02 at low temperatures. (b) Incremental resistivity $\Delta\rho(x,T)=\rho(x,T)-\rho(0,T)$ vs. $T^2$ of $Th_{1-x}U_x$ alloys with $x=0.005$, 0.01 and 0.02. After Ref. [19].

ductors under pressure for a postdoctoral research physicist, T. Fred Smith. I benefited from the advice of Prof. Jon Olsen of ETH, Zürich, an expert in high-pressure studies of superconductors, who was visiting the Matthias group during the 1963–1964 academic year. He referred me to the famous paper of Chester and Jones [31] in which the 'clamped' piston–cylinder high-pressure cell was described. I designed a piston–cylinder clamp device that was constructed in the UCSD campus machine shop and later used by Fred Smith to perform a beautiful series of measurements of the pressure dependence of $T_c$ of a number of interesting superconducting materials including elements, such as Re and U, and the A15 compounds, the class of superconductors with the highest $T_c$'s prior to the advent of the cuprates. The clamp device I designed (overdesigned!) was so massive and robust that it served as the principal research tool for the Ph.D. thesis research of several graduate students in Matthias' group and, later, my own group, and is still used today!

### *4.1. Dilute rare earth systems*

In the late 1960s, I employed the piston–cylinder clamp technique to study several superconductors containing Ce impurities: $La_3In$ [32], La [33] and $LaAl_2$ [34]. Measurements of the AC magnetic susceptibility of the systems $La_{3-x}Ce_xIn$ and $La_{1-x}Ce_x$ under pressure in the 20 kbar range, performed in collaboration with Kang-Soo Kim, revealed that the Ce impurities, which were magnetic and produced a Kondo effect at atmospheric pressure, appeared to undergo a continuous demagnetization under pressure. We inferred this from the behavior of the pressure dependence of the rate of depression of $T_c$ by the Ce additions which initially increased, passed through a maximum, and then decreased. This is illustrated in Fig. 8 which shows $T_c$ vs. pressure for the system $La_{1-x}Ce_x$ with several concentrations $x$ of Ce. The $T_c(P)$ data above 20 kbar were derived from resistivity measurements under pressure using the Bridgman anvil technique in collaboration with Jörg Wittig, a postdoctoral research physicist from Germany, who was visiting the Matthias group at the time. The data for the $La_{1-x}Ce_x$ sample with $x=0.02$ are particularly striking; the application of pressure drives $T_c$ to zero at about 5 kbar, $T_c$ remains zero up to ~15 kbar, whereupon superconductivity reappears and $T_c$ increases with pressure. These results can be interpreted in terms of an increase of $T_K$, and, in turn, the ratio $T_K/T_{co}$, with pressure. As $T_K/T_{co}$ increases under pressure, the initial depression of $T_c$ with $x$ is expected to increase, pass through a maximum, and then decrease, according the theory of MHZ [25]. However, at the highest pressures, such large values of $T_K$ are required (~$10^6$ K!) that we concluded that the Ce 4f state must demagnetize within the context of the Friedel–Anderson model. In later work, we

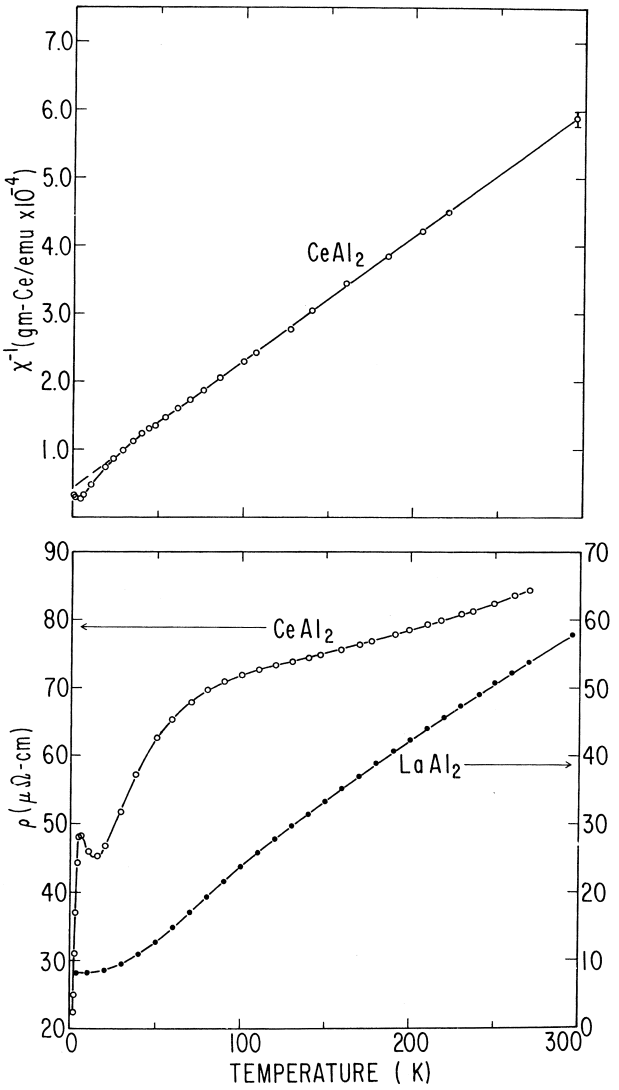


Fig. 7. Inverse magnetic susceptibility $\chi^{-1}$ vs. temperature for $CeAl_2$ (upper panel) and electrical resistivity $\rho$ vs. temperature for $CeAl_2$ and a $LaAl_2$ reference (lower panel). After Ref. [27].

found that a similar demagnetization of the Ce 4f state occurs in the $La_{1-x}Ce_x$ system when Th is substituted for La. With increasing Th concentration $y$ in the $(La_{1-y}Th_y)_{1-x}Ce_x$ system, the rate of the initial depression of $T_c$ with Ce concentration passes through a pronounced maximum and $T_c$ vs. $n$ changes continuously from curves with negative curvature and reentrant behavior to curves with positive curvature and exponential-like shapes [14]. Concomitantly, the normal state magnetic susceptibility [35] and electrical resistivity [36] evolve continuously from magnetic to non-magnetic behavior. A self-consistent analysis of the rates of the initial depression of $T_c$ with $n$ and the value of the specific heat jump at $T_c$ showed that the MHZ theory provides a good description of the data from $T_K/T_{co} \approx 0.1$ to $10^2$ [37,38].

We independently confirmed the increase of $T_K$ with pressure inferred from the behavior of the depression of $T_c$ with pressure through measurements of the normal state electrical resistivity as a function of pressure for the $La_{1-x}Ce_x$ [39] and $Y_{1-x}Ce_x$ [40] systems.

### 4.2. Concentrated rare earth systems

In 1971, Dieter Wohlleben and I developed a technique for performing magnetization measurements on weakly magnetic materials using the Faraday method in conjunction with small clamped high-pressure cells that could be suspended from a microbalance in an inhomogeneous magnetic field [41]. We employed this technique in a number of investigations including the pressure-induced demagnetization of Ce metal [42] and SmS [43], discussed in the following, and the effect of pressure on the magnetization and Curie temperature of the weak ferromagnets $ZrZn_2$ [44] and UPt [45].

#### 4.2.1. Pressure-induced demagnetization of a one-electron 4f shell in a metal

We first applied the technique we had developed for making magnetic measurements under pressure using the Faraday method to Ce metal. We measured the magnetic susceptibility $\chi$ of Ce at room temperature vs. pressure $P$ up to ~18 kbar through the hysteretic $\gamma$–$\alpha$ phase transition that occurs at ~8 kbar with increasing pressure and then at ~10 kbar in the $\alpha$-phase as a function of temperature between ~0.4 K and room temperature [42]. The $\chi(P)$ data at room temperature exhibited a sharp decrease (increase) in $\chi$ at ~8 kbar (~6 kbar) with increasing (decreasing) pressure, while the $\chi$ vs. $T$ data at ~10 kbar displayed Pauli-like behavior, reflecting the non-magnetic character of $\alpha$-Ce. This experiment provided a direct demonstration of the pressure-induced demagnetization of a *one-electron* 4f shell in a concentrated rare earth metallic system. Also, we noted that the valence of the non-magnetic $\alpha$-phase of Ce is +3.7 at room temperature, according to estimates by Gschneidner and Smoluchowski [46] and Franceschi and Olcese [47].

#### 4.2.2. Pressure-induced demagnetization of a many-electron 4f shell in a metal

After we had completed our $\chi(P)$ measurements on Ce metal, we became aware of a paper by Jayaraman et al. [48] in which it was reported that the compound SmS undergoes a similar discontinuous and hysteretic transition under pressure at ~6.5 kbar (~1.5 kbar) with increasing (decreasing) pressure from a semiconducting 'black' phase to a metallic 'gold' phase [49]. The transition was accompanied by a large decrease in volume ($\Delta V/V \sim -8\%$) without change in the NaCl crystal structure. In the low-pressure semiconducting phase, the Sm ions are divalent and electrical conductivity occurs via thermal activation of localized electrons from the Sm 4f electron shells into the conduction band with a small activation energy of ~0.2 eV [50]. The Sm 4f electron shell contains six electrons and

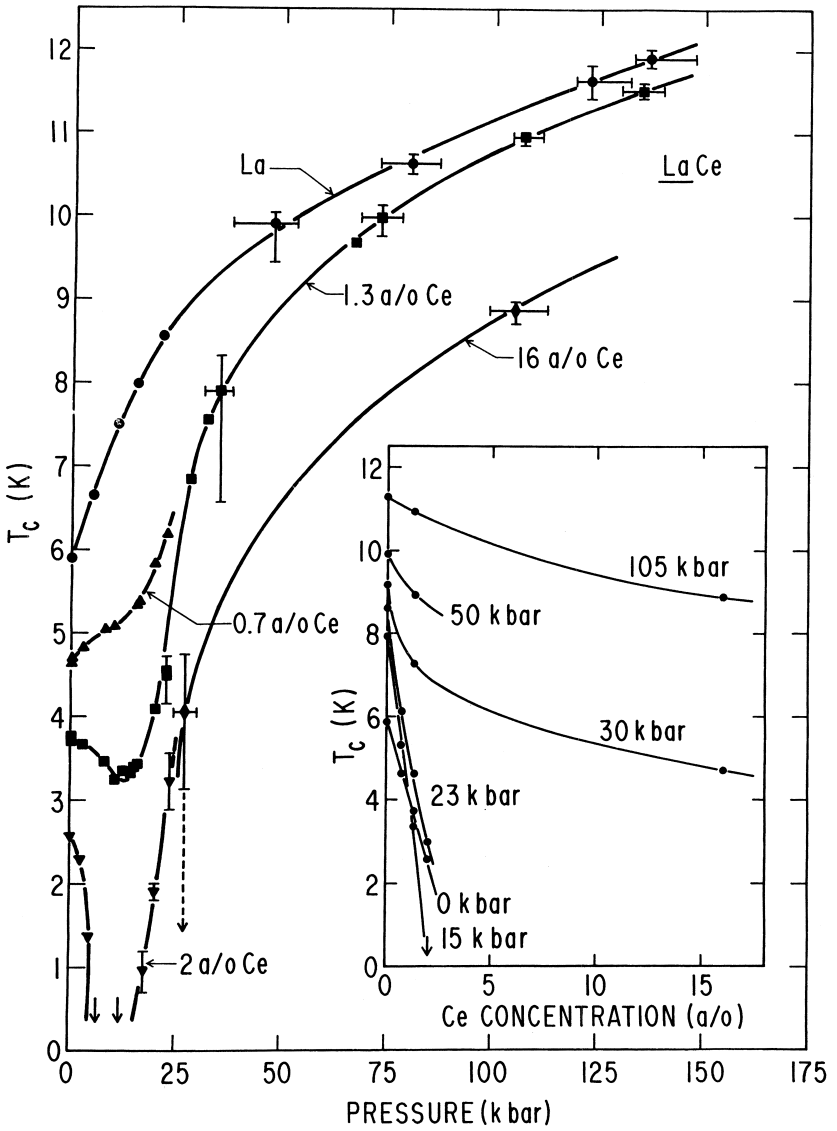


Fig. 8. Superconducting critical temperature $T_c$ vs. pressure for the $La_{1-x}Ce_x$ system. Isobars of $T_c$ vs. Ce concentration are shown in the inset. After Ref. [33].

the compound exhibits ionic Van Vleck paramagnetism with a non-magnetic $J=0$ ground state. Jayaraman et al. [48] concluded that the pressure-induced semiconductor–metal transition in SmS (as well as SmSe and SmTe, in which the transition is a continuous function of pressure) and the pressure–volume relationship are consistent with the conversion of $Sm^{2+}$ to $Sm^{3+}$.

We reasoned that if the electronic phase transition in SmS involves the promotion of an electron from the 4f shell into the conduction band, the material would become metallic and the five electrons remaining in the 4f shell would carry a localized magnetic moment, resulting in a Curie–Weiss law and, presumably, some type of magnetic order at low temperatures, according to Kramer's theorem. What we found was quite surprising; the magnetic susceptibility of SmS in its collapsed 'gold' phase is only weakly temperature dependent, indicating that the Sm ions are non-magnetic in the high-pressure phase [43]. This experiment constituted the first demonstration of the pressure-induced demagnetization of a *many-electron* 4f shell in a concentrated rare earth metallic system. It revealed that, in a metallic environment, the magnetic moment of a rare earth ion can be as unstable as that of transition metal ion! Shown in Fig. 9 are room temperature $\chi$ vs. $P$ data for SmS in which the sharp drop in $\chi$ at the hysteretic phase transition from the insulating low-pressure phase to the collapsed 'gold' phase is clearly evident. Displayed in Fig. 10 are $\chi$ vs. $T$ data at atmospheric pressure and above 10 kbar which show that $\chi$ exhibits weakly $T$-dependent Pauli-like behavior in the collapsed 'gold' phase.

At about the same time, the compound $SmB_6$ was found to show non-magnetic behavior at atmospheric pressure which was attributed to the Sm ions undergoing a transition to a divalent state at low temperature [51]. In

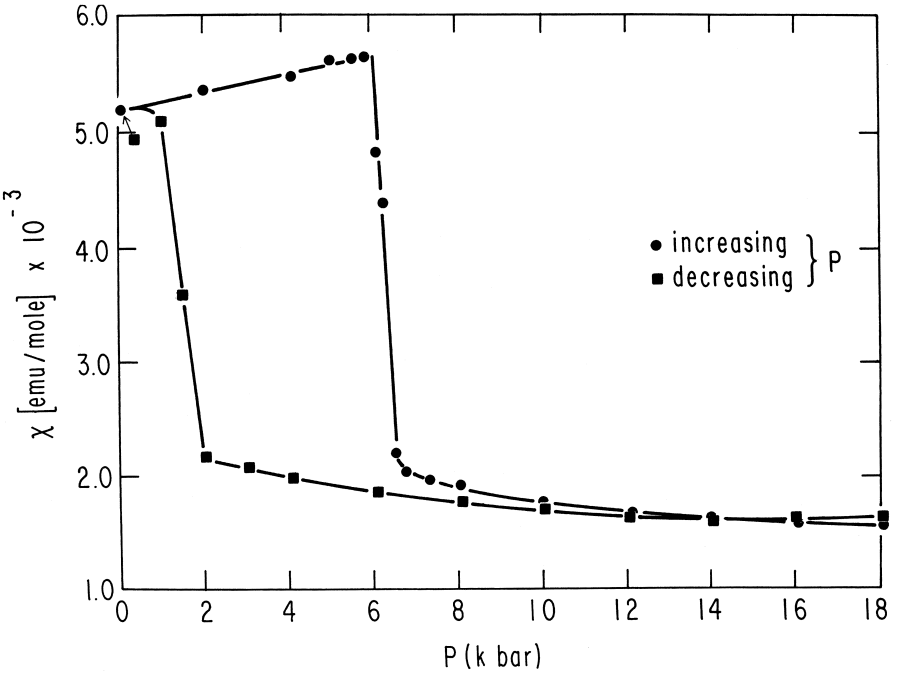


Fig. 9. Magnetic susceptibility $\chi$ vs. pressure $P$ for SmS at room temperature. After Ref. [43].

subsequent studies, it was determined that the Sm ions have two configurations, $4f^6$ and $4f^5$, in the fixed ratio $4f^6$:$4f^5 \approx 3:7$, which was ascribed to the rigidity of the B lattice [52].

*4.2.3. Valence fluctuations of rare earth ions in metals*

Based on the non-magnetic behavior and intermediate valence of Ce metal and SmS in their collapsed high-pressure phases and $SmB_6$ at atmospheric pressure, we

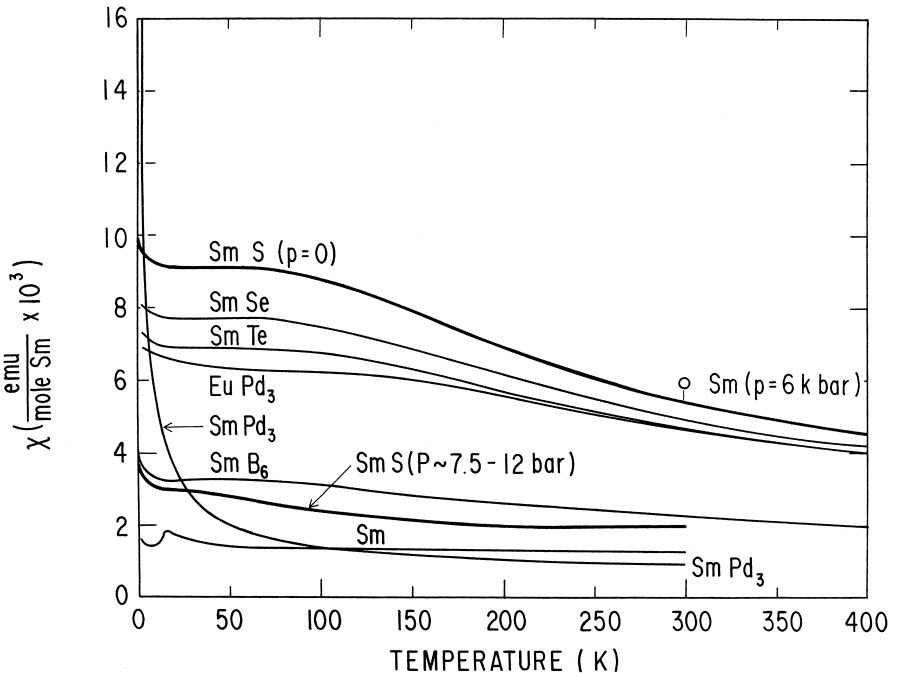


Fig. 10. Magnetic susceptibility $\chi$ of SmS at zero pressure and in its high-pressure collapsed metallic phase vs. temperature. Also shown for comparison are $\chi(T)$ data for compounds with the configuration $4f^6$ (SmSe, SmTe and $EuPd_3$), the configuration $4f^5$ (Sm and $SmPd_3$), and the intermediate valence compound $SmB_6$. After Ref. [43].

pointed out a striking correlation between the three materials [43,53]: (i) The R ion in all three materials has an unusual intermediate valence. (ii) All three materials are non-magnetic in the sense that there is no indication of a local moment near 0 K, and the susceptibility decreases weakly with increasing temperature above a characteristic temperature of the order of 100 K.

We also noted that the fractional valence, $\varepsilon = (a_n - a_{n+\varepsilon})/(a_n - a_{n+1})$, where $a_n$ is the lattice constant for $n$ valence electrons, was about 70% for all three materials. In the case of $SmB_6$, this value was corroborated by Mössbauer isomer shift [54] and soft X-ray absorption [55] measurements. We suggested that the 'collapsed' phase of $SmB_6$ happens to be stable at atmospheric pressure, and that Sm ions in $SmB_6$ at atmospheric pressure and in SmS above 6.5 kbar are essentially in the same state. In an attempt to find a common mechanism which would stabilize the valence at an intermediate value over a substantial range of pressure and temperature, we proposed [43,53] a phenomenological 'valence fluctuation' or 'inter-configuration fluctuation' model in which the R ion exhibits temporal fluctuations between two states with integral valence, or, equivalently, two 4f electron shell configurations, $4f^n$ and $4f^{n-1}$ (+conduction electron). The typical valence fluctuation frequency $f$ is expected to be roughly given by $f \sim k_B T_o/h$, where $T_o$ is a characteristic temperature that separates non-magnetic behavior at low temperatures $T \ll T_o$ from local moment behavior at high temperatures $T \gg T_o$.

We suggested that for temperatures much larger than $T_o$, the magnetic susceptibility can be approximated by an expression of the form:

$$\chi(T) \sim N\{\varepsilon(n)[\mu_{\text{eff}}(n)]^2 + [1-\varepsilon(n)][\mu_{\text{eff}}(n-1)]^2\}/3k_B(T+T_o) \quad (4)$$

where $N$ is the number of R ions, $\varepsilon(n)$ is the fraction of time the configuration $4f^n$ is occupied, and $\mu_{\text{eff}}(n)$ is the effective magnetic moment associated with the configuration $4f^n$. For temperatures much smaller than $T_o$, the susceptibility should approach a finite value as $T \to 0$; i.e.:

$$\chi(T) \to \text{constant as } T \to 0 \quad (5)$$

rather than diverging as a Curie law or undergoing a transition to a magnetically ordered state. The non-magnetic behavior below the characteristic temperature $T_o$ is accompanied by Kondo-like anomalies in the physical properties near $T_o$, such as a resistance minimum followed by a large increase in resistivity as the temperature is lowered, and peaks in the specific heat and thermoelectric power. This striking behavior originates from the unstable valence of certain R ions and, phenomenologically, is qualitatively similar in both concentrated and dilute R metallic systems.

Additional evidence for intermediate valence of Sm in the collapsed phase of SmS was provided by Mössbauer isomer shift measurements on SmS in the high-pressure collapsed metallic phase and the chemically collapsed pseudobinary compound $Sm_{0.77}Y_{0.23}S$ [56], and X-ray photoemission spectroscopy (XPS) studies on various chemically collapsed pseudobinary compounds formed by alloying SmS with a third element [57]. Whereas the Mössbauer isomer shift measurements were unable to resolve the presence of the two Sm 4f electron shell configurations, $4f^6$ and $4f^5$, in the high-pressure and chemically collapsed metallic phases of SmS, the XPS measurements revealed their simultaneous presence in chemically collapsed metallic SmS. Within the context of the valence fluctuation (VF) model, this is consistent with a characteristic VF lifetime of $\sim 5\times 10^{-13}$ s, since the measuring time is $\sim 10^{-9}-10^{-7}$ s for the Mössbauer isomer shift measurements and $\sim 10^{-17}$ s for the XPS measurements.

This correlation between intermediate valence and non-magnetic behavior prompted us to look for other intermediate valence compounds and determine whether they were non-magnetic. With Brian Sales, who was then a young graduate student in Matthias' group, we identified a number of intermediate valence rare earth compounds from their lattice constants and measured their magnetic susceptibility. We were pleased to discover that these materials were also non-magnetic, as illustrated by the $\chi$ vs. $T$ data for several Yb compounds with intermediate valence shown in Fig. 11 [53]. The phenomenological model was developed further by Sales and Wohlleben [58] who showed that it could provide a quantitative description of $\chi(T)$ for a number of intermediate valence rare earth compounds.

Subsequently, it was found that SmS, in its collapsed 'gold' phase, and $SmB_6$ are actually semiconductors with very small energy gaps $\Delta \sim$several meV. This small gap semiconducting behavior was attributed to hybridization between the localized 4f and conduction electron states [59]. Later, in the mid-1980s, we found that the filled skutterudite compounds $CeFe_4P_{12}$ and $UFe_4P_{12}$ exhibited semiconducting behavior with energy gaps $\Delta \sim 0.1$ eV which correlated with intermediate valence, at least in the case of $CeFe_4P_{12}$ [60,61]. These compounds were the first Ce- and U-based analogues of the Sm-based semiconductors, 'gold' SmS and $SmB_6$. In the mean time, many other rare earth and uranium compounds have been found that show this 'hybridization gap semiconductor' or 'Kondo insulator' behavior, and interest in this problem has been rekindled [62].

## 5. Magnetically ordered superconductors

In the mid-1970s, two systems of ternary rare earth compounds, the rare earth molybdenum chalcogenides, $RMo_6X_8$ (X=S, Se) [63,64], and the rare earth rhodium borides, $RRh_4B_4$ [65], were discovered. These compounds

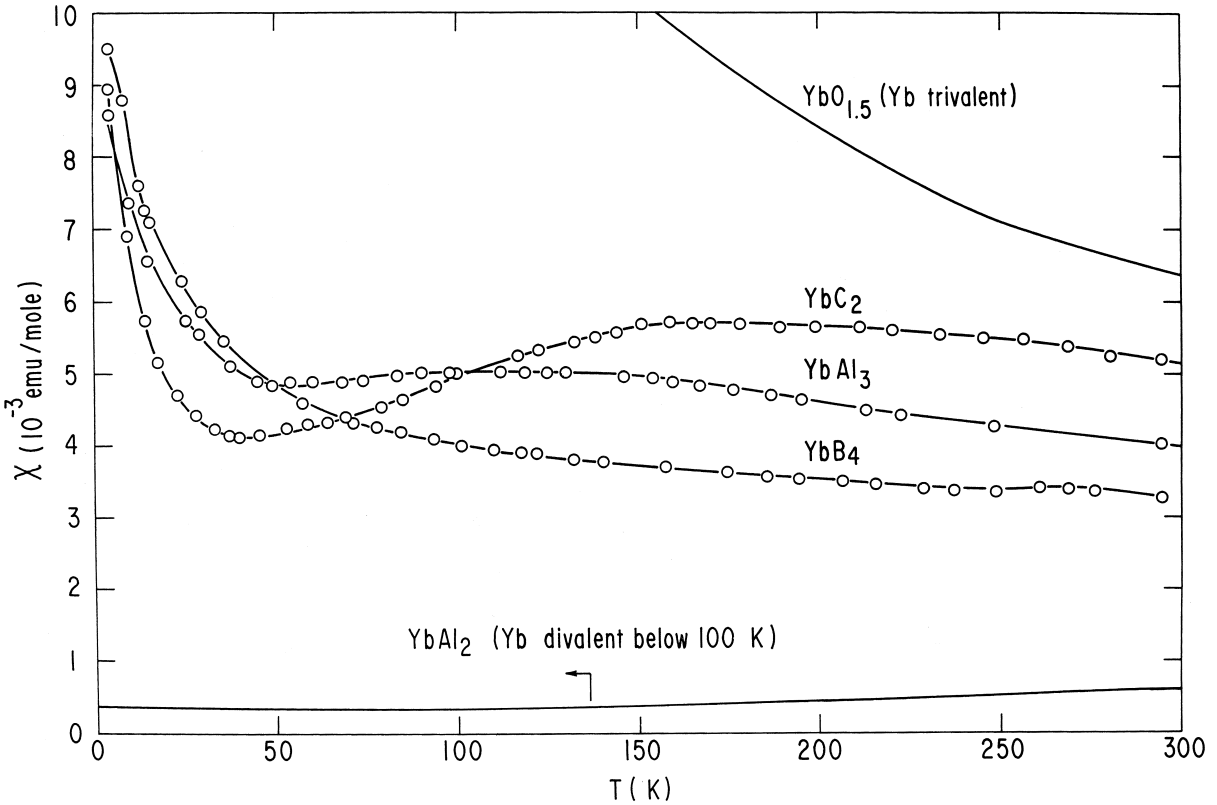


Fig. 11. Magnetic susceptibility $\chi$ vs. temperature $T$ for several non-magnetic Yb compounds with intermediate valence. After Ref. [53].

contain an ordered sublattice of magnetic R ions, but are, nevertheless, superconducting, making it possible to investigate experimentally the interplay between superconductivity and long-range magnetic order [66,67]. The occurrence of superconductivity, even in the presence of relatively large concentrations of R ions, has been attributed to the crystal structures of these materials which are comprised of transition metal clusters and R ions. The superconductivity appears to be associated primarily with the transition metal 4d electrons which interact only weakly with the R ions. For these investigations, R ions whose localized 4f-electron states are not appreciably hybridized with conduction electron states were selected so that they would have well defined magnetic moments and the exchange interaction parameter $\mathcal{J}$ would be small, yielding two interpenetrating and weakly interacting subsystems, one of which is superconducting and the other of which is magnetically ordered.

### *5.1. Antiferromagnetic superconductors*

The coexistence of superconductivity and long-range antiferromagnetic (AFM) order was discovered in the latter part of the 1970s in the R molybdenum selenides $RMo_6Se_8$ (R=Gd, Tb and Er) [67,68] and R rhodium borides $RRh_4B_4$ (R=Nd, Sm and Tm) [67,69] at UCSD, and in the R molybdenum sulfides $RMo_6S_8$ (R=Gd, Tb, Dy and Er) [67,70] at the University of Geneva. The occurrence of AFM ordering of the R magnetic moments in the superconducting state was inferred from a $\lambda$-type anomaly in the specific heat and a cusp in the magnetic susceptibility for the $RMo_6Se_8$ compounds [67,68] and from a feature in the upper critical field $H_{c2}$ vs. temperature $T$ curve in the $RMo_6S_8$ compounds [67,70]. Neutron diffraction measurements on $GdMo_6Se_8$ [71] and $RMo_6S_8$ compounds with R=Gd, Tb and Dy [72] confirmed the AFM ordering of the sublattice of R ions in the Chevrel phase structure.

Shown in Fig. 12 are resistively determined $H_{c2}$ vs. $T$ curves for the non-magnetic superconductor $LuRh_4B_4$, the AFM superconductors $NdRh_4B_4$ and $SmRh_4B_4$, and the ferromagnetic superconductor $ErRh_4B_4$ [73]. These data indicate that there is no universal behavior of $H_{c2}(T)$ for AFM superconductors; both enhancements and depressions of $H_{c2}$ are found below the Néel temperature $T_N$, which appear to be determined by a combination of different mechanisms [74]. The $H_{c2}(T)$ curve of $SmRh_4B_4$ is enhanced in the AFM state over that in the paramagnetic state and has a sharp break in slope at $T_N=0.87$ K [75,76]. In contrast, the $H_{c2}$ vs. $T$ curve of $NdRh_4B_4$, which undergoes two AFM transitions at $T_{N1}=1.31$ K and $T_{N2}=0.89$ K, decreases abruptly at $T_{N1}$ and then increases sharply at $T_{N2}$ [69,76]. Neutron diffraction experiments indicate that the magnetic phases of $NdRh_4B_4$ in zero magnetic field are body-centered tetragonal AFM structures in which the $Nd^{3+}$ moments are alternately aligned parallel and antiparallel to the $c$-axis, with a sinusoidal

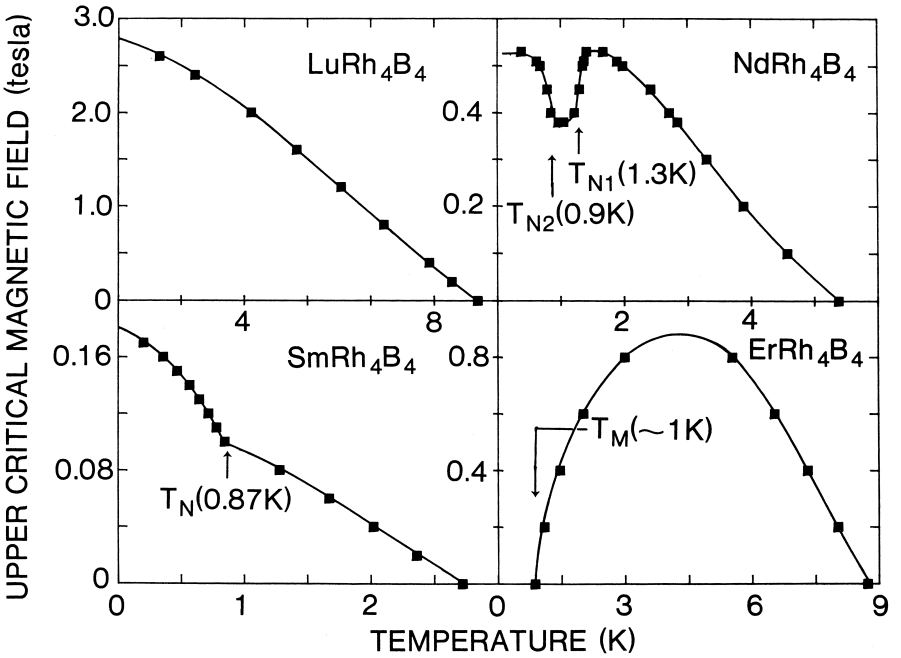


Fig. 12. Resistively determined upper critical field vs. temperature for polycrystalline samples of the non-magnetic superconductor $LuRh_4B_4$, the antiferromagnetic superconductors $NdRh_4B_4$ and $SmRh_4B_4$, and the ferromagnetic superconductor $ErRh_4B_4$. After Ref. [73].

modulation along the [100] direction with $\lambda = 46.5$ Å in the high-temperature magnetic phase, and along the [110] direction with $\lambda = 45.2$ Å in the low-temperature magnetic phase [77]. For the AFM superconductor $TmRh_4B_4$, the $H_{c2}$ vs. $T$ curve (not shown in Fig. 12) hardly changes at $T_N = 0.4$ K [76,78].

Recently, the coexistence of superconductivity and AFM order was observed in several $RNi_2B_2C$ compounds [79,80]. Another class of materials in which the coexistence of superconductivity and antiferromagnetism occurs are high-$T_c$ cuprates containing R ions such as the $RBa_2Cu_3O_{7-\delta}$ and $Ln_{2-x}M_xCuO_{4-y}$ compounds [81].

### 5.2. Ferromagnetic superconductors

Reentrant superconductivity due to the onset of long-range ferromagnetic (FM) ordering of the R magnetic moments was discovered in 1977 in $ErRh_4B_4$ [82] at UCSD, and in $HoMo_6S_8$ [83] at the University of Geneva. These two materials, which become superconducting at an upper critical temperature $T_{c1}$, lose their superconductivity at a lower critical temperature $T_{c2} \approx \theta_c$, where $\theta_c$ is the Curie temperature. Thermal hysteresis in various physical properties and a spike-shaped feature in the specific heat near $T_{c2}$ indicate that a first-order transition from the superconducting to the FM normal state occurs at $T_{c2}$ [67]. Typical AC magnetic susceptibility and electrical resistance vs. temperature data for $ErRh_4B_4$ are displayed in Fig. 13 [84]. The thermal hysteresis at $T_{c2}$ in both properties is evident. The resistively determined $H_{c2}$ vs. $T$ curve for $ErRh_4B_4$ is shown in Fig. 12 [76,85].

Neutron diffraction measurements have confirmed that $ErRh_4B_4$ [86,87] and $HoMo_6S_8$ [88] have FM ground states. In addition, small angle neutron scattering studies of $ErRh_4B_4$ [87,89] and $HoMo_6S_8$ [90] revealed the existence of a sinusoidally modulated magnetic state with a wavelength of the order of $10^2$ Å that coexists with superconductivity in a narrow temperature interval above $T_{c2}$. The neutron diffraction measurements of Moncton et al. [87] on polycrystalline $ErRh_4B_4$ showed that the FM transition is broad, extending up to ~1.4 K, well above $T_{c2}$ and into the superconducting state, and that there is marked thermal hysteresis between ~0.8 K and ~1.4 K. The width of the FM transition was attributed to a distribution of effective Curie temperatures within the material, while the hysteresis was ascribed to the nucleation of normal FM domains within the paramagnetic superconducting regions between $T_{c2}$ and ~1.4 K [87]. Thus, the regions within which superconductivity and the sinusoidally modulated magnetic state coexist appear to be interspersed with normal FM domains to form a spatially inhomogeneous state. Shown in Fig. 14 are specific heat data in the vicinity of $T_{c2}$ taken by introducing heat pulses while the average sample temperature drifted upward (warming) and while it drifted downward (cooling) [91–93]. The data also revealed thermal hysteresis, part of which appears to be associated with the formation of FM domains, discussed above in connection with the neutron scattering experiments (between ~0.9 K and ~1.3 K), and part of which is due to the reentrant transition at $T_{c2}$. Subsequent neutron scattering experiments on an $ErRh_4B_4$ single crystal by Sinha et al. [89] confirmed the results of the earlier neutron scattering

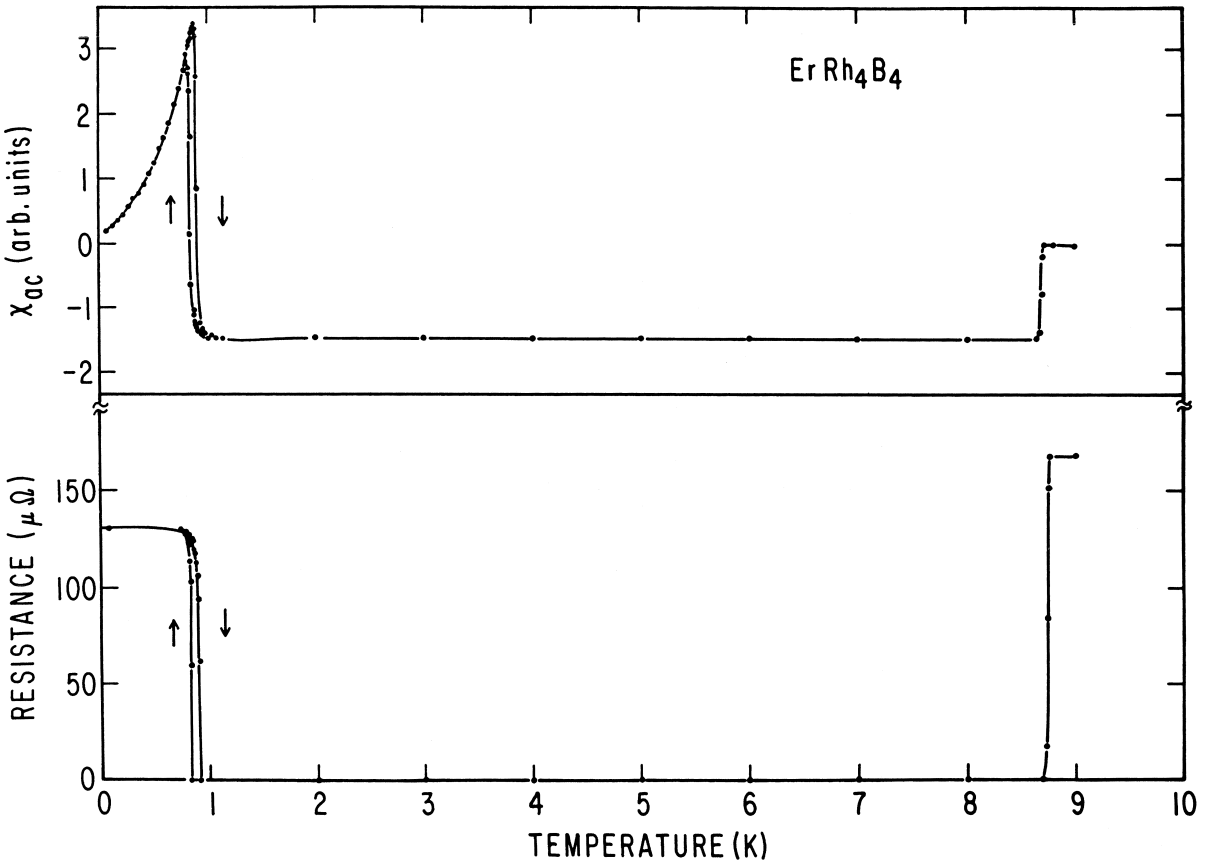


Fig. 13. Typical AC magnetic susceptibility $\chi_{ac}$ and electrical resistance vs. temperature data for $ErRh_4B_4$. After Ref. [84].

studies of Moncton et al. [87] on polycrystalline $ErRh_4B_4$ and further revealed that the sinusoidally modulated magnetic state is a transverse linearly polarized long-range magnetic state with a wavelength of ~100 Å. The linearly polarized sinusoidal modulation lies along the [010] axis and the propagation directions are at 45° to the [001] and the [100] axes.

The sinusoidally modulated magnetic state that coexists with superconductivity in $HoMo_6S_8$ and $ErRh_4B_4$ is reminiscent of the cryptoferromagnetic state proposed by Anderson and Suhl in 1959 in a theory based on the exchange interaction [94]. A number of other theories, involving the electromagnetic interaction, were developed in the late 1970s and early 1980s to account for the sinusoidally modulated magnetic state, such as those of Blount and Varma [95], Ferrell et al. [96], and Matsumoto et al. [97]. Although the exchange interaction is operative in these materials, the electromagnetic interaction appears to be primarily responsible for the sinusoidally modulated magnetic state that coexists with superconductivity. Other possibilities for the periodic magnetic structure above $T_{c2}$ that have been considered are: (i) a spontaneous vortex lattice; (ii) a laminar structure, stabilized by the R magnetization in a self-consistent manner; and (iii) combined spiral magnetic and spontaneous vortex states [74,98].

### *5.3. Superconductivity and competing magnetic interactions*

Experiments on pseudoternary R compounds provide an alternative method for studying the interaction between superconductivity and long-range magnetic order, as well as for exploring the effects of competing types of magnetic moment anisotropy and/or magnetic order. Two types of $RRh_4B_4$ pseudoternaries have been formed, one in which a second R element is substituted at the R sites, and another in which a different transition element is substituted at the Rh sites.

An interesting example, which belongs to the first type of pseudoternary $RRh_4B_4$ system, is $(Er_{1-x}Ho_x)Rh_4B_4$ whose low-temperature phase diagram, delineating the paramagnetic, superconducting, and magnetically ordered phases, is shown in Fig. 15. The phase boundaries have been determined from AC magnetic susceptibility measurements [99,100] and neutron diffraction experiments [101]. The phase diagram displays regions in which the $Er^{3+}$ and $Ho^{3+}$ magnetic moments independently order ferromagnetically within the basal plane and along the tetragonal *c*-axis, respectively, separated by a region of mixed magnetic phases. The temperature interval above $T_{c2}$ within which the sinusoidally modulated magnetic

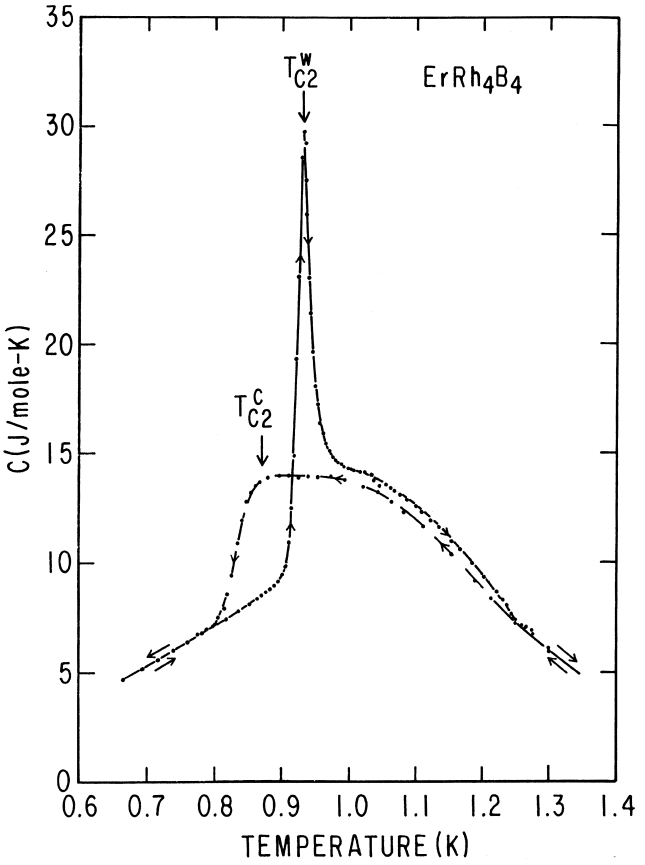


Fig. 14. Specific heat of $ErRh_4B_4$, measured upon warming and cooling, in the vicinity of the reentrant superconducting–normal transition at $T_{c2}$. The arrows denoted $T^{w}_{c2}$ and $T^{c}_{c2}$ represent the values of $T_{c2}$ determined from AC magnetic susceptibility measurements made upon warming and cooling, respectively. After Ref. [91–93].

phase in $ErRh_4B_4$ coexists with normal FM domains is also indicated in Fig. 15. This inhomogeneous phase presumably persists within a certain region in the $T$–$x$ plane (shaded area in the figure). There is a tricritical point at the concentration $x_c = 0.89$ where $T_{c1}$, $T_{c2}$ and $T_M$ become coincident. The $T_{c2}$ vs. $x$ phase boundary is depressed relative to a linear extrapolation to $x < x_c$ of $T_M$ vs. $x$ for $x > x_c$ (dashed curve in Fig. 15). Analysis of neutron diffraction data on a $(Er_{0.4}Ho_{0.6})Rh_4B_4$ sample [102] indicates that the actual $T_M$ of 3.67 K is about 0.2 K less than it would have been in the absence of superconductivity, in accord with the dashed-line extrapolation as well as theoretical predictions.

## 6. Heavy fermion materials

Heavy fermion materials are rare earth and actinide compounds in which the linear coefficient $\gamma$ of the electronic specific heat ($C_e = \gamma T$) has an enormous value that can be as high as several J mol$^{-1}$ K$^{-2}$, corresponding to a large electron effective mass $m^* \sim 10^2$–$10^3 m_e$, where $m_e$ is the free electron mass [73,103–106]. The origin of the heavy fermion state is believed by many researchers to be associated with the Kondo effect. In several of these compounds, antiferromagnetism and superconductivity coexist with $T_N > T_c$ ($UPt_3$, $URu_2Si_2$, $UNi_2Al_3$, $UPd_2Al_3$) [105]. Recently, a crossover with decreasing temperature from localized moment behavior to heavy Fermi liquid behavior was found in the metallic compound $LiV_2O_4$ [107]. At $T = 1$ K, the $\gamma$ value of ~0.42 J mol$^{-1}$ K$^{-2}$ is

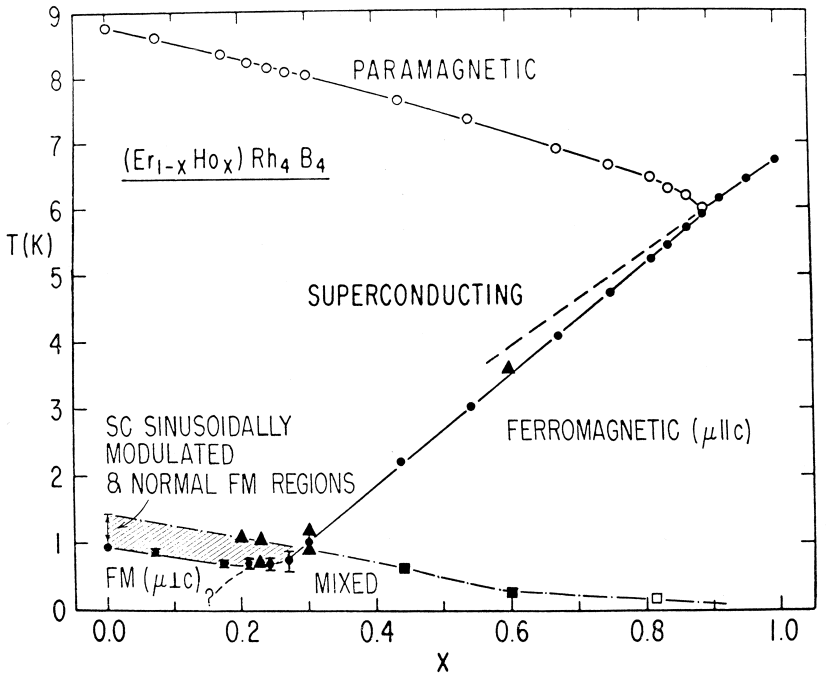


Fig. 15. Temperature–composition ($T$–$x$) phase diagram for the $Er_{1-x}Ho_xRh_4B_4$ pseudoternary system. After Ref. [99].

exceptionally large for a transition metal compound and comparable to that of f-electron heavy fermion compounds such as $UPt_3$.

The small group of heavy fermion superconductors includes one Ce compound, $CeCu_2Si_2$ [108], and five U compounds, $UBe_{13}$ [109], $UPt_3$ [110], $URu_2Si_2$ [111], $UNi_2Al_3$ [112] and $UPd_2Al_3$ [113], listed in the order in which they were discovered. These materials apparently exhibit an unconventional type of anisotropic superconductivity in which the superconducting energy gap $\Delta(\boldsymbol{k})$ vanishes at points or on lines on the Fermi surface, and the electron pairing may be mediated by AFM spin fluctuations. Evidence for anisotropic superconductivity includes power-law temperature dependences of various physical properties, such as ultrasonic attenuation, spin lattice relaxation rate, thermal conductivity, and magnetic field penetration depth, in the superconducting state.

### *6.1. The compound $UPd_2Al_3$*

An interesting heavy fermion compound that will be discussed in a different context in Section 7.2 is $UPd_2Al_3$. This compound has an electron effective mass $m^* \approx 50 m_e$, inferred from the value $\gamma \approx 140$ mJ mol$^{-1}$ K$^{-2}$ [114], and exhibits AFM order with a Néel temperature $T_N = 14.6$ K and superconductivity that coexists with the AFM order below $T_c \approx 2$ K [113]. The AFM state consists of an AFM stacking along the *c*-axis of FM planes of relatively large ordered moments of $0.85\mu_B$ lying in the hexagonal basal plane [115]. The isotropic reduction of the Knight shift below $T_c$ indicates singlet spin pairing of electrons in the superconducting state, while the $T^3$ dependence of the spin lattice relaxation rate $T_1^{-1}$ at low temperatures suggests a d-wave pairing state with a line of nodes around the *c*-axis [116,117]. Recent electron tunneling measurements on epitaxial thin films of $UPd_2Al_3$ revealed a feature in the tunneling differential conductivity vs. voltage curve at ~1.2 meV that has been attributed to AFM spin fluctuations [118], since this energy is close to a 1.5 meV gapped dispersive spin excitation at the magnetic Bragg point $Q = (0,0,1/2)$ that has been observed in inelastic neutron scattering experiments [119,120] and is well below the characteristic phonon energy $E_{ph} \sim k_B \Theta_D \sim 13$ meV corresponding to a Debye temperature $\Theta_D \approx 150$ K. Strong coupling between magnetism and superconductivity has also been inferred from the neutron scattering studies [119,120].

### *6.2. The compound $UBe_{13}$ and the system $U_{1-x}Th_xBe_{13}$*

An example of the dramatic difference between the superconducting properties of heavy fermion compounds and those of conventional superconductors is illustrated in Fig. 16 which contains a plot of the upper critical field $H_{c2}$ vs. $T$ of $UBe_{13}$ [121]. The magnitude of the initial slope of $H_{c2}(T)$, ~42 T K$^{-1}$, is the largest ever reported for a bulk superconductor. The $H_{c2}(T)$ curve has an extremely unusual shape with a linear region that persists to very low temperatures. An analysis of the $H_{c2}(T)$ curve near $T_c$ in terms of the conventional theory of type II superconductivity indicates that the magnitude of the initial slope $(-dH_{c2}/dT)_{Tc}$ is consistent with a quasiparticle effective mass $m^* \sim 300 m_e$.

Particularly interesting behavior is observed when Th is substituted for U to form the system $U_{1-x}Th_xBe_{13}$ whose low-temperature $T$–$x$ phase diagram is shown in Fig. 17 [106,122,123]. With increasing $x$, $T_c$ exhibits a nearly linear decrease with $x$ with a distinct minimum at $x \approx 0.017$, a broad maximum at $x \approx 0.03$, and a subsequent decrease of $T_c$ [122]. For compositions $x$ between ~0.017 and ~0.04, two features have been observed in the specific heat, the upper one associated with the development of the superconducting state and the lower one corresponding to another phase transition that occurs without destroying the superconductivity [123]. Further evidence for multiple phase transitions in the range $0.017 < x < 0.04$ has been provided by μSR measurements which reveal a broadening of the relaxation rate below the second transition [124]. The lower temperature phase could be a superconducting phase with a complex order parameter that breaks time-reversal symmetry or a purely magnetic phase with a small magnetic moment $\sim 10^{-3}$–$10^{-2}\mu_B$ that coexists with superconductivity.

The results of measurements of $T_c(P)$ on the $U_{1-x}Th_xBe_{13}$ system made in our laboratory are displayed in Fig. 18 as isobars of $T_c$ vs. $x$ for $0 \le x \le 12$ kbar [125]. Two different types of behavior are present for each pressure, separated by the minimum in $T_c(x)$ at $x_{min}$. For $x < x_{min}$, a monotonic decrease of $T_c(x)$ is observed as the pressure increases, and the magnitude of the slope $dT_c/dP$ also becomes larger with increasing $x$. For $x > x_{min}$, an abrupt increase of $T_c$ occurs with a maximum and subsequent decrease for higher $x$. The position of this maximum is pressure dependent, moving to higher concentration as $P$ increases. It is tempting to infer from the $T_c(x)$ curves the existence of two distinct superconducting phases, one in the region $0 \le x \le x_{min}$ (which we refer to as type A) and the other at $x > x_{min}$ (type B), where $x_{min}$ is a function of pressure. The way the $T_c(x)$ curves evolve with pressure suggests that the $T_c(x)$ phase boundary for $x < x_{min}$ extends approximately linearly with the same slope into the region $x > x_{min}$.

### *6.3. The compound $UPt_3$*

The other heavy fermion superconductor which exhibits multiple superconducting phases is $UPt_3$. This system has been investigated extensively and more complete discussions can be found in several recent reviews [126–128]. The most definitive evidence for the existence of two distinct superconducting transitions was provided by specific heat measurements which, in zero magnetic field,

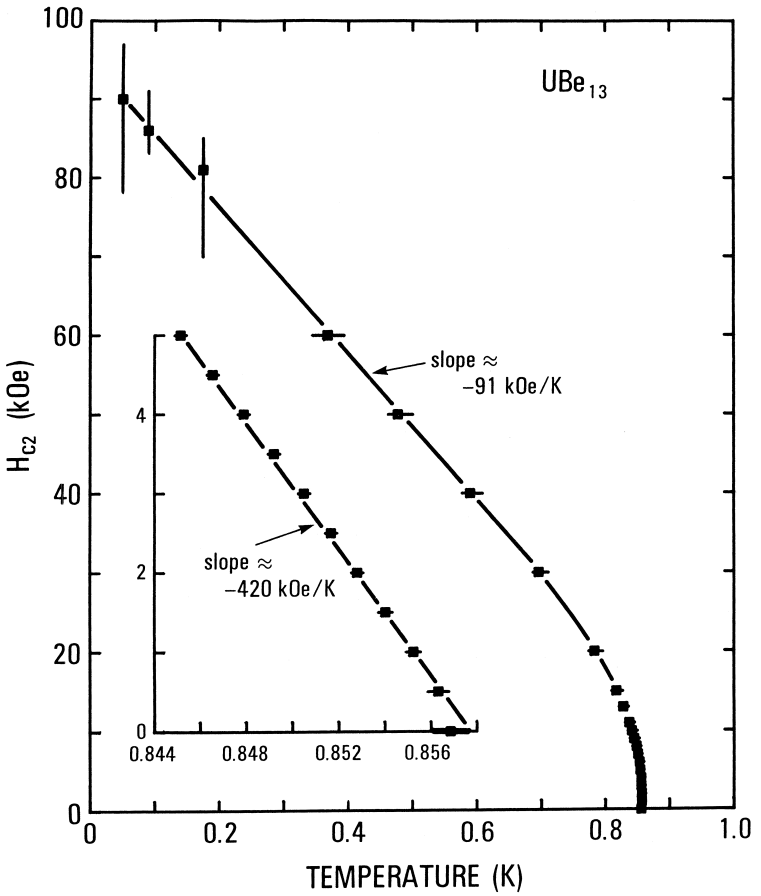


Fig. 16. Upper critical field $H_{c2}$ vs. temperature for the heavy fermion compound $UBe_{13}$. The inset shows $H_{c2}(T)$ near $T_c$. After Ref. [121].

reveal two specific heat jumps, one at a critical temperature $T_{c1}$ and the other at a critical temperature $T_{c2}$, about 50 mK below $T_{c1}$ [129]. Specific heat measurements in magnetic fields applied perpendicular to the $c$-axis of a $UPt_3$ single crystal made by Hasselbach et al. [130] showed that the two superconducting transitions converge with increasing field and coalesce into a single transition above ~0.5 T. These and other measurements such as ultrasonic attenuation have been used to construct an $H$–$T$ phase diagram which has three different superconducting phases and a tetracritical point for both $H \perp c$ and $H \| c$ [126]. The occurrence of the two superconducting transitions has been attributed to the coupling between a multicomponent superconducting order parameter and the AFM order parameter [128]. The two superconducting transitions in $UPt_3$ are also very sensitive to applied pressure and merge into a single transition at a pressure of ~3.7 kbar, above which only a single transition is observed [131,132].

The two zero-field phases, which are often denoted as A and B for the high- and low-temperature phases, respectively, have different superconducting characteristics. Point contact spectroscopy reveal a gap-like feature in the B-phase which is not present in the A-phase [133]. Zero-field μSR measurements indicate an increase in internal magnetic field in the B-phase [134]. Measurements of the relaxation of the remanent magnetization of magnetic vortices in superconducting $UPt_3$ show that there are striking differences in the low-field flux dynamics between the A- and B-phases [135]. In the low-temperature B-phase, the logarithmic creep rate is practically zero, while in the high-temperature A-phase, it is finite and increases rapidly as the temperature is increased towards $T_{c1}$. It was speculated that the reduced bulk creep rate in the B-phase may be due to time-reversal symmetry breaking in this phase, wherein fractional vortices become trapped on walls between domains of degenerate superconducting phases [135].

Some of the strongest evidence for anisotropic superconductivity in $UPt_3$ comes from ultrasonic attenuation measurements in the superconducting state on single crystals by Shivaram et al. [136]. For the propagation vector of the ultrasound wave in the basal plane of $UPt_3$, the ultrasonic attenuation coefficient $\alpha$ was found to vary as $\sim T$ for the polarization $\boldsymbol{e} \| \boldsymbol{a}$ and $\sim T^3$ for $\boldsymbol{e} \| \boldsymbol{c}$. In the normal state, the same dependence of $\alpha$ on $T$ was observed for both $\boldsymbol{e} \| \boldsymbol{a}$ and $\boldsymbol{e} \| \boldsymbol{c}$.

The depression of $T_c$ of $UPt_3$ by rare earth, Th, and Zr substitutions for U was investigated in our laboratory in 1995 [137]. The results are shown in Fig. 19 in which the

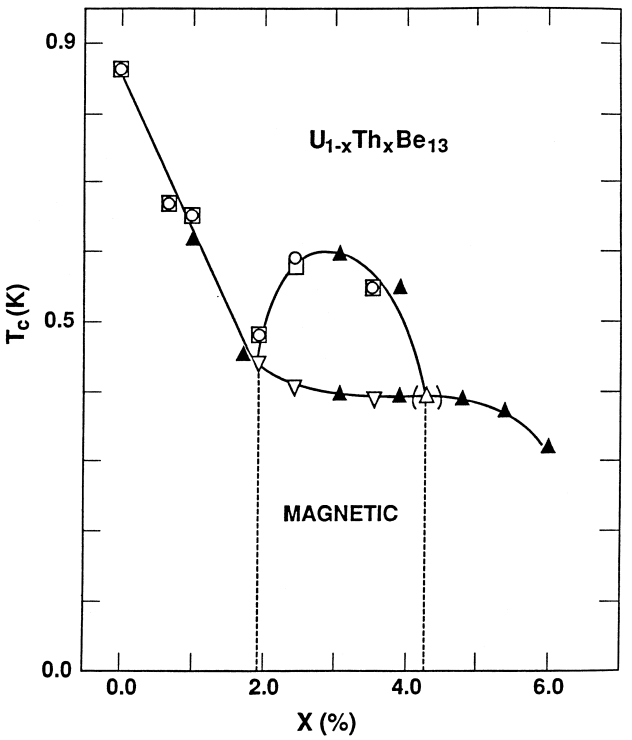


Fig. 17. Temperature–composition ($T$–$x$) phase diagram for $U_{1-x}Th_xBe_{13}$ determined from various measurements: AC magnetic susceptibility (squares), magnetization (circles), kink in lower critical field (inverted triangles), and specific heat (solid upright triangles). After Ref. [106].

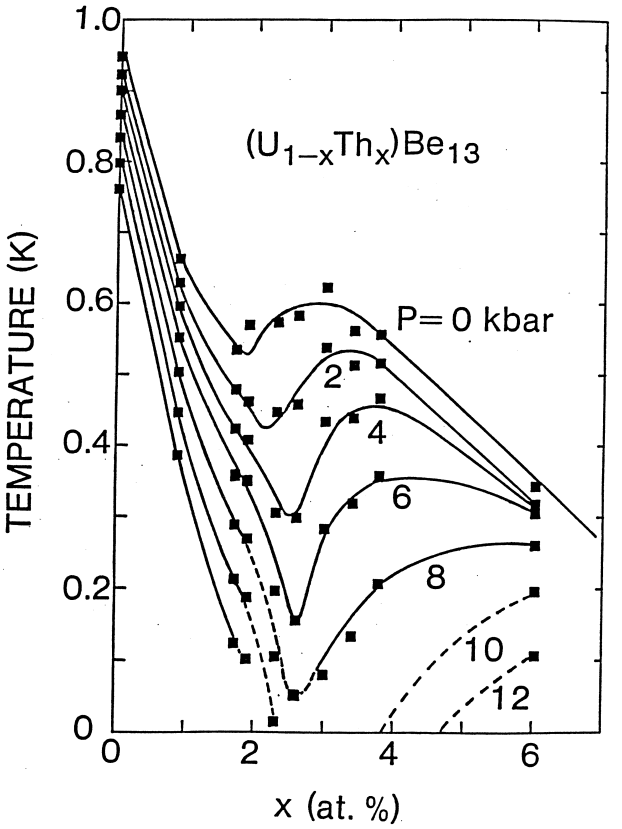


Fig. 18. Isobars of the superconducting critical temperature $T_c$ vs. $x$ for $U_{1-x}Th_xBe_{13}$ between 0 and 12 kbar. After Ref. [125].

depression of $T_c$, $T_{co}-T_c$, for a series of $U_{0.997}R_{0.003}Pt_3$ compounds, where R = rare earth (except Pm and Lu), Th and Zr, is plotted vs.: (a) R ionic radius; and (b) residual resistivity $\rho_o$. The linear increase of the depression of $T_c$ with increasing residual resistivity indicates that the primary pair breaking mechanism is impurity potential scattering, rather than exchange scattering. While the scaling of $T_{co}-T_c$ with residual resistivity is strong evidence for anisotropic superconductivity in $UPt_3$, the absence of a marked correlation of the depression of $T_c$ with the deGennes factor of the rare earth ion suggests that the superconducting order parameter in the A-phase of $UPt_3$ has odd parity. Other evidence for odd parity of the Cooper pairs in $UPt_3$ include: (i) Pt NMR and μSR Knight shift measurements [138–140]; and (ii) Pt NMR Knight shift measurements throughout the multiple superconducting phases in the $H$–$T$ plane for major magnetic field directions [141].

### *6.4. The compound $URu_2Si_2$ and the systems $URu_{2-x}M_xSi_2$ ($M$ = Re,Tc)*

The moderately heavy electron compound $URu_2Si_2$ provides a striking example of the coexistence of superconductivity and AFM order with $T_N > T_c$. Shown in Fig. 20 are plots of $C/T$ vs. $T^2$ and $\delta C$ vs. $T$ (inset), where $\delta C(T) = C(T) - (\gamma T + \beta T^3)$ for $URu_2Si_2$ [142]. We noted that: (i) the specific heat anomaly $\delta C$ associated with the 17.5 K transition in $URu_2Si_2$ has a shape that is reminiscent of a second-order BCS-type mean field transition and can be described by the relation $\delta C = A\exp(-\Delta/T)$ with an activation energy $\Delta \approx 130\ \mathrm{K} \approx 11$ meV; and (ii) the value of the electronic specific heat coefficient $\gamma$ extrapolated to 0 K (65.5 mJ mol$^{-1}$ K$^{-2}$) is substantially reduced with respect to the value of $\gamma$ at temperatures above 17.5 K (112 mJ mol$^{-1}$ K$^{-2}$). On the basis of these observations and the types of anomalies found in the electrical resistivity and the magnetic susceptibility of $URu_2Si_2$ near 17.5 K, we proposed that a charge density wave (CDW) or spin density wave (SDW) transition may occur at 17.5 K that opens up a gap of ~11 meV over about 40% of the Fermi surface. According to neutron scattering experiments on a $URu_2Si_2$ single crystal, the 17.5 K transition is due to an AFM phase with a (100) modulation wave vector and spins along the tetragonal $c$-axis [143]. Although the ordered moment is small (~$0.03\mu_B$), intense, propagating and longitudinal spin waves with a zone center gap of 1.8 meV were observed which coexist with the superconducting phase below $T_c$.

The effects of pressure [144] and transition metal substitution for Ru [145] on the superconducting and SDW transition in polycrystalline samples of $URu_2Si_2$ have been investigated. The inverse correlation of the pressure depen-

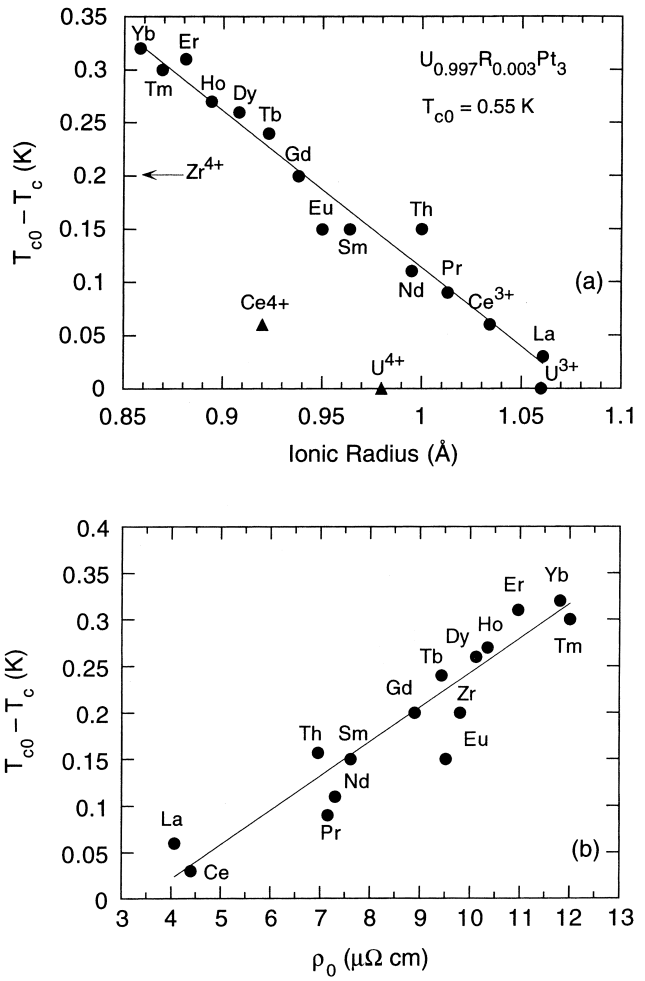


Fig. 19. (a) Depression of the superconducting critical temperature $T_c$, $T_{co} - T_c$, vs. R ionic radius for $U_{0.997}R_{0.003}Pt_3$ compounds where R = lanthanide (except Pm and Lu), Th and Zr. $T_{co}$ is the superconducting critical temperature of $UPt_3$. (b) $T_{co} - T_c$ vs. residual resistivity for the same compounds as in (a). After Ref. [137].

dences of $T_N$ and $T_c$ is consistent with an increase of the fraction of the Fermi surface that is removed by the formation of the SDW state as a function of pressure. If an increase of $T_N$ is associated with an increase in the fraction of electron states involved in the formation of the SDW, rather than an increase in the coupling constant, then a smaller number of electron states would be available for pairing, leading to a decrease in $T_c$. Small additions of chemical substitutions also reveal an inverse correlation between $T_c$ and $T_N$, again reflecting the competition between superconductivity and the SDW for the Fermi surface. However, in addition, the disorder associated with the chemical substitution rapidly suppresses and broadens the superconducting and AFM transitions. The substitution of Th for U is particularly effective in suppressing the specific heat anomalies associated with both the AFM and superconducting transitions [146]. It has been suggested [146] that this could be related to pair breaking effects due to 'Kondo holes' as non-magnetic Th is substituted into the superconducting $URu_2Si_2$ matrix.

Another common behavior that is emerging for superconducting heavy fermion uranium compounds is that chemical substitutions tend to suppress both superconductivity and weak AFM order and induce local moment AFM order or FM order with moments of the order of a $\mu_B$. In $UPt_3$, local moment antiferromagnetism is produced by substituting Th for U [147,148] and Pd [149] or Au [150] for Pt, while in $URu_2Si_2$, local moment antiferromagnetism appears upon substitution of Rh for Ru [151] and local moment ferromagnetism occurs when Re or Tc is substituted for Ru [152], the first example of a FM instability in a heavy electron system. The FM state in $URu_{2-x}M_xSi_2$ (M = Re, Tc) solid solutions occurs in the Re or Tc solute range $0.4 < x < 1.4$ with maximum magnetic moments of $0.44\mu_B$/U atom at $x \approx 0.8$ for Re and $0.27\mu_B$/U atom at $x \approx 1$ for Tc. The saturation moment $\mu_s$, Curie temperature $\theta_c$, effective moment $\mu_{eff}$, and coefficient of the electronic specific heat $\gamma$ as a function of composition $x$ in the $URu_{2-x}M_xSi_2$ (M = Re, Tc) systems are shown in Fig. 21 [152].

## 7. Non-Fermi liquid behavior in f-electron materials

During the past decade, there has been growing interest in non-Fermi liquid (NFL) behavior in strongly correlated f-electron materials [153]. The NFL behavior is manifested as weak power-law and logarithmic divergences in temperature in the physical properties of these materials at low temperatures. This new class of NFL materials is comprised of certain intermetallic compounds containing Ce, U or Yb ions that carry magnetic dipole or electric quadrupole moments which interact with the spins and charges of the conduction electrons and can undergo magnetic or quadrupolar ordering at low temperatures. The NFL behavior was first established in chemically substituted f-electron compounds containing non-magnetic substituents [154,155], although NFL behavior has recently been observed in several stoichiometric f-electron compounds as well [156,157].

For many of the f-electron systems, $\rho(T)$, $C(T)$ and $\chi(T)$ have the following NFL temperature dependences for $T \ll T_o$: (i) $\rho(T) \sim 1 - a(T/T_o)^n$ where $|a| \approx 1$, $a < 0$ or $> 0$, and $n \approx 1 - 1.5$; (ii) $C(T)/T \sim (-1/T_o)\ \ln(T/T_o)$, or $\sim T^{-1+\lambda}$; and (iii) $\chi(T) \sim 1 - (T/T_o)^{1/2}$, $\sim (-1/T_o)\ \ln(T/T_o)$, or $\sim T^{-1+\lambda}$. In several of the f-electron systems, the characteristic temperature $T_o$ can be identified with the Kondo temperature $T_K$. These new NFL f-electron materials can be compared with 'conventional' heavy fermion f-electron compounds, such as $CeAl_3$ and $UPt_3$, which behave as Fermi liquids [158], in spite of the strong electron–electron interactions that renormalize the electron mass by $\sim 10^2$–$10^3$! (Or, equivalently, the effective Fermi

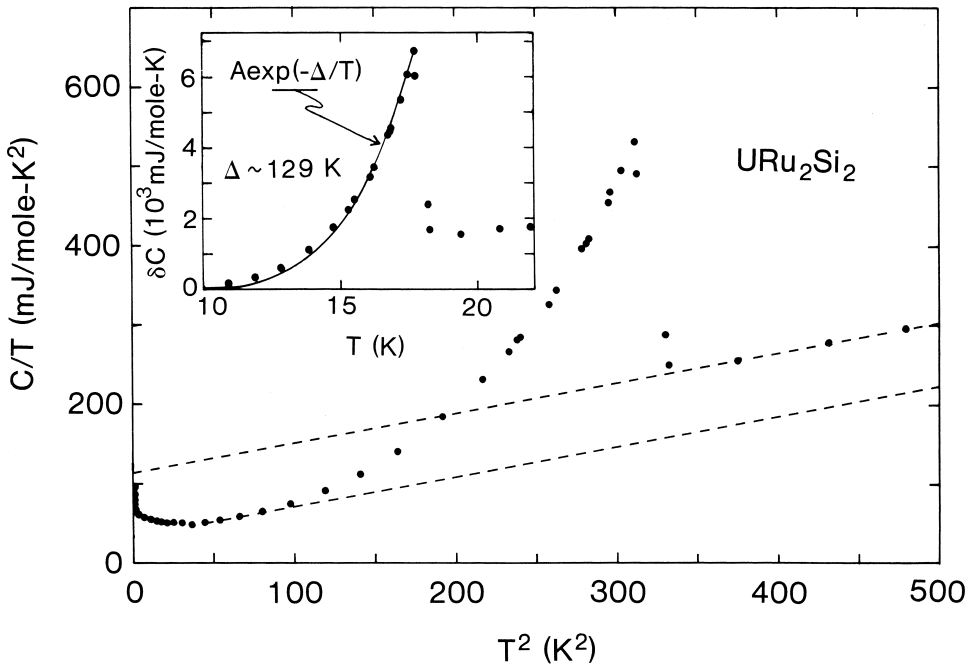


Fig. 20. Specific heat $C$, plotted as $C/T$ vs. $T^2$, for $URu_2Si_2$. Shown in the inset is the magnetic contribution $\delta C$ vs. $T$; the line represents a fit of the relation $\delta C = A\exp(-\Delta/T)$ to the data, yielding the value $\Delta \sim 129$ K for the energy gap. After Ref. [142].

temperature $T_F$ is low, ~1–10 K!) Here, the temperature and frequency dependences of the physical properties scale with $T_F$. The quantities $\rho(T)$, $C(T)$ and $\chi(T)$ have the following familiar forms for $T \ll T_F$: (i) $\rho(T) \sim 1 - a(T/T_F)^2$, where $|a| \approx 1$, $a > 0$ or $< 0$; (ii) $C(T)/T \sim \gamma_o$, where $\gamma_o$ can be as large as ~several J mol$^{-1}$ K$^{-2}$!; and (iii) $\chi(T) \sim \chi_o$, such that $\chi_o/\gamma_o \sim 1$.

Experiments on a variety of f-electron systems suggest that there are two routes to NFL behavior in these materials, a single ion route involving an unconventional Kondo effect and a interionic interaction route associated with order parameter fluctuations in the vicinity of a second-order magnetic (or, possibly, quadrupolar) phase transition that has been suppressed to zero temperature (quantum critical point). Theoretical models based on single ion physics include a multichannel Kondo effect, of either magnetic or electric (quadrupolar) origin [159–163] and a conventional Kondo effect with a distribution of Kondo temperatures due to chemical disorder (referred to as the Kondo disorder model) [164,165]. Theoretical models which incorporate interionic interactions include fluctuations of an order parameter in the vicinity of a second-order phase transition at 0 K [166–172] and an inhomogeneous Griffiths' phase [173]. The Griffiths' phase consists of magnetic clusters in a paramagnetic phase and forms as a result of the competition between the Kondo effect and the Ruderman–Kittel–Kasuya–Yosida (RKKY) interaction in the presence of magnetic anisotropy and disorder. Most of the chemically substituted systems in which NFL behavior is found have rich phase diagrams that contain regions where there is magnetic order, quadrupolar order, spin glass freezing, Kondo effect coupled with low-temperature NFL behavior, heavy Fermi liquid behavior, and superconductivity. The proximity of the glassy or long-range ordered magnetic phases to the phases with Kondo and low-temperature NFL behavior has made it difficult to distinguish between single ion or cooperative effects as the source of the NFL behavior.

### *7.1. The $Y_{1-x}U_xPd_3$ system*

In 1990, we discovered an unconventional Kondo effect with concomitant NFL behavior at low temperatures in the $Y_{1-x}U_xPd_3$ system for U concentrations $x$ in the range $0 \leq x \leq 0.2$ [174,175]. The most recent version of the low-temperature–composition ($T$–$x$) phase diagram of the $Y_{1-x}U_xPd_3$ system is shown in Fig. 22 [176]. Within the U concentration interval $0 < x \leq 0.5$, where $Y_{1-x}U_xPd_3$ crystallizes in the cubic $Cu_3Au$ structure, three different ground states are found: NFL behavior ($0 < x \lesssim 0.2$), spin glass freezing ($0.2 \lesssim x \lesssim 0.42$), and long-range AFM order ($0.42 \lesssim x \lesssim 0.5$). As indicated in Fig. 21, the Kondo temperature $T_K$ decreases rapidly with $x$. This has been attributed to 'Fermi level tuning,' a phenomenon in which the $U^{4+}$ 5f binding energy $\varepsilon_f = E_F - E_f$, where $E_F$ is the Fermi energy and $E_f$ is the energy of the $U^{4+}$ 5f state, increases by ~1 eV as $x$ increases from 0 to 1 [177,178]. The increase of $\varepsilon_f$ with $x$ was discovered in photoemission studies of $Y_{1-x}U_xPd_3$ [179] and can be understood in terms of the increase of $E_F$ with $x$ as tetravalent U is substituted for trivalent Y. The nearly linear increase of $\varepsilon_f$ with $x$ should cause a rapid decrease in $T_K$ since:

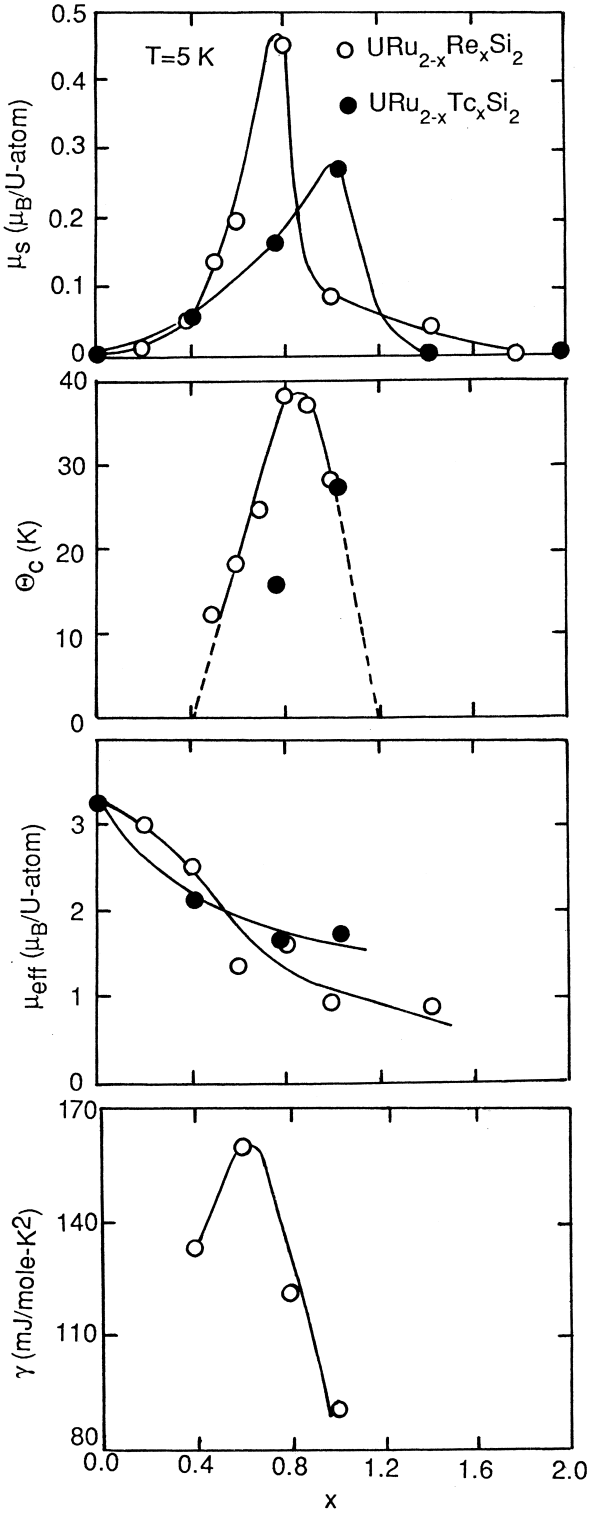


Fig. 21. Saturation moment $\mu_s$, Curie temperature $\theta_c$, effective magnetic moment $\mu_{eff}$, and electronic specific heat coefficient $\gamma$ as a function of composition $x$ in $URu_{1-x}Re_xSi_2$ and $URu_{1-x}Tc_xSi_2$ compounds. After Ref. [152].

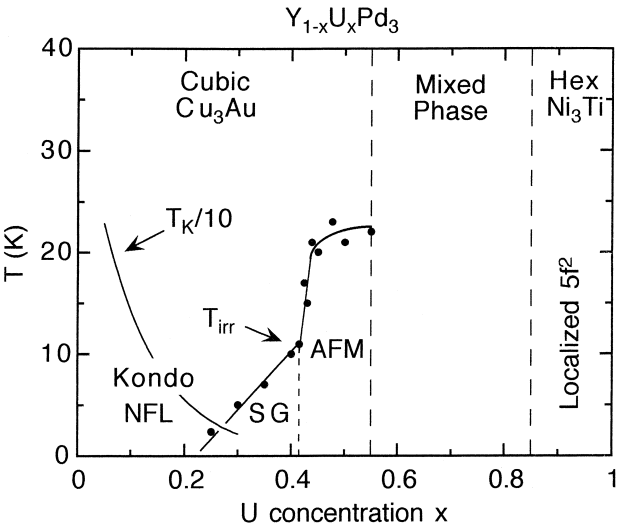


Fig. 22. Temperature–composition ($T$–$x$) phase diagram for the $Y_{1-x}U_xPd_3$ system. Antiferromagnetic (AFM), spin glass (SG), Kondo, and non-Fermi liquid (NFL) regimes are identified in the figure. The meaning of the symbols are: $T_{irr}$, irreversibility temperature; $T_K$, Kondo temperature. After Ref. [176].

$$T_K \sim T_F \exp[-1/N(E_F)|\mathcal{J}|]$$
$$\sim T_F \exp[-\varepsilon_f/ < V_{kf}^2 > N(E_F)] \quad (6)$$

where $T_F$ is the Fermi temperature, $N(E_F)$ is the density of states at $E_F$, $\mathcal{J} \sim -\langle V_{kf}^2 \rangle / \varepsilon_f$ is the exchange interaction parameter, and $V_{kf}$ is the hybridization matrix element.

An analysis of the NFL characteristics in $\Delta\rho(T)$, $\Delta C(T)$ and $\Delta\chi(T)$, the U contributions to $\rho(T)$, $C(T)$ and $\chi(T)$, indicates that these features scale with U concentration $x$ and Kondo temperature $T_K$, where $T_K$ is inferred from the high-temperature behavior of $\rho(T)$ and $\chi(T)$, at least over the range $0.1 \leq x \leq 0.2$. It has proven to be difficult to test the scaling of $\Delta\rho(T)$, $\Delta C(T)$ and $\Delta\chi(T)$ to lower values of $x$ as the NFL features weaken rapidly with decreasing $x$ since their magnitudes are proportional to $x$ and their gradients decrease with increasing $T_K$ (decreasing $x$). Examples of the striking NFL characteristics in $\Delta\rho(T)$, $\Delta C(T)$ and $\Delta\chi(T)$ at low temperatures that are found in the $Y_{1-x}U_xPd_3$ system are shown in Figs. 23(a)–(c), respectively.

The $\Delta\rho(T)$ data displayed in Fig. 23(a) have been fitted using the relation $\Delta\rho(T)/\Delta\rho(0) = 1 - a(T/T_K)^n$, where $\Delta\rho(0)$ and $n$ are adjustable fitting parameters. Since the best fit yields the value $n = 1.1 \pm 0.1$, we conclude that the $\Delta\rho(T)$ data are consistent with the expression:

$$\Delta\rho(T)/\Delta\rho(0) = 1 - a(T/T_K) \quad (7)$$

The $\Delta C(T)/T$ data shown in Fig. 23(b) can be described well by an expression of the form:

$$\Delta C(T)/T = (-bR/T_K) \ln[b'(T/T_K)] \quad (8)$$

in the range $0.3\ K < T \leq 10\ K$, but deviate from it below

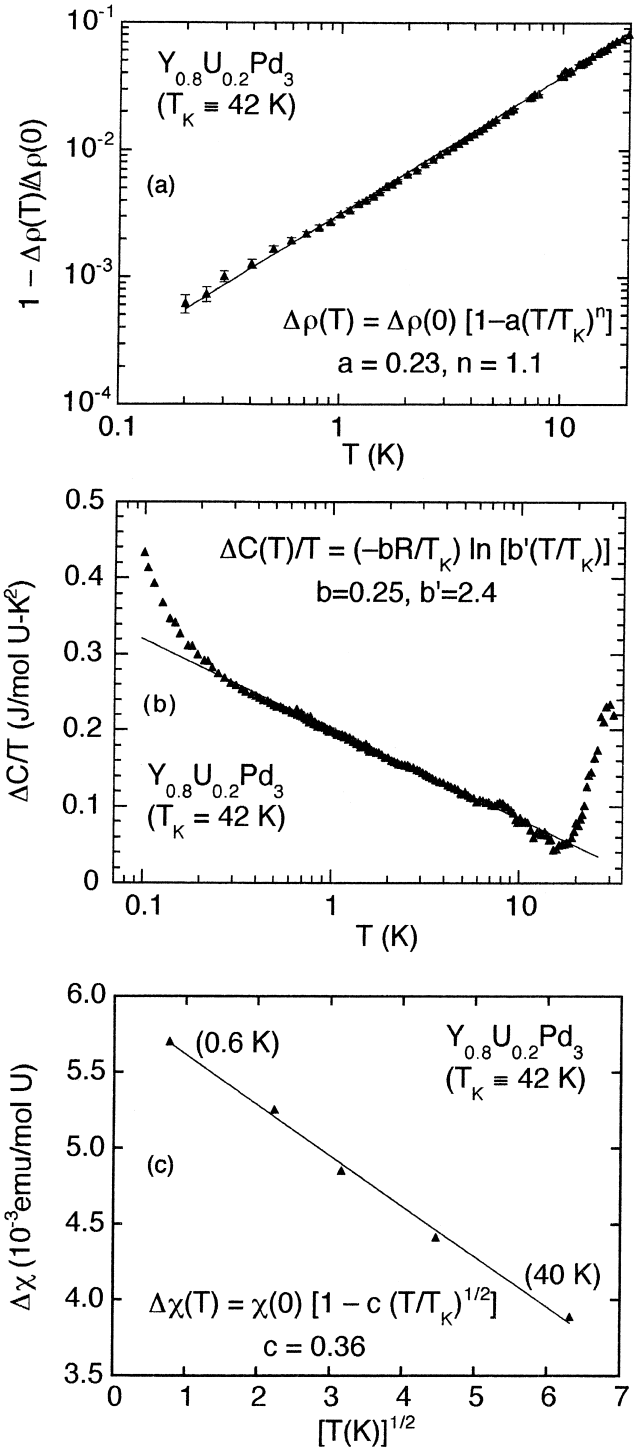


Fig. 23. The U contribution to the electrical resistivity, $\Delta\rho$, specific heat, $\Delta C$, and magnetic susceptibility, $\Delta\chi$, of $Y_{0.8}U_{0.2}Pd_3$, plotted as: (a) $\log[1-\Delta\rho(T)/\Delta\rho(0)]$ vs. $\log T$; (b) $\Delta C(T)/T$ vs. $\log T$; and (c) $\Delta\chi(T)$ vs. $T^{1/2}$. After Ref. [176].

0.3 K. Within the context of a two-channel spin−1/2 Kondo model, this upturn in $\Delta C(T)/T$ could be due to a lifting of the degeneracy of a $U^{4+}$ doublet ground state by an exchange field or the CEF, which could remove the residual $(R/2)\ln(2)$ entropy. The $\Delta\chi(T)$ data in Fig. 23(c) can be fitted between 0.6 K and 40 K by an expression of the form:

$$\Delta\chi(T)/\Delta\chi(0) = 1 - c(T/T_K)^{1/2} \quad (9)$$

after the magnetization $M(H,T)$ data have been corrected by removing a non-linear contribution that scales with $H/(T-\theta_p)$ and was assumed to be due to magnetic impurities [177]. The constants $a$, $b$, $b'$ and $c$ that appear in Eqs. (7)–(9) are of the order of unity and were determined from an analysis described in Ref. [176].

The scaling of $\Delta\rho(T)$, $\Delta C(T)$ and $\Delta\chi(T)$ with $x$ and $T_K$ suggests that the NFL behavior at low temperatures is a single ion phenomenon that is associated with the Kondo effect observed at higher temperatures. A single ion quadrupolar Kondo model, the electric analogue of the magnetic two-channel spin−1/2 Kondo model, can account for some of the NFL features. According to this model, the electrical resistivity $\Delta\rho(T)$ should vary as $\Delta\rho(T)/\Delta\rho(0) = 1 - a(T/T_K)^{1/2}$ [162], a result that is clearly at variance with the experimentally observed linear $T$ dependence described by Eq. (7). On the other hand, the quadrupolar Kondo model predicts that the specific heat $\Delta C(T)$ [160,180] and the magnetic susceptibility $\Delta\chi(T)$ [181] have the same forms as Eqs. (8) and (9), respectively, both of which are consistent with experiment [154,177,178]. Furthermore, the applicability of the quadrupolar Kondo model to the $Y_{1-x}U_xPd_3$ system requires that the ground state of $U^{4+}$ in the cubic crystal CEF be the $\Gamma_3$ non-magnetic doublet which carries an electric quadrupole moment. (In a cubic CEF, the nine-fold degenerate $J=4$ Hund's rule multiplet of $U^{4+}$ is split into $\Gamma_4$ and $\Gamma_5$ triplets, a $\Gamma_1$ singlet, and a $\Gamma_3$ non-magnetic doublet.) Several inelastic neutron scattering (INS) experiments have been carried out in an effort to determine the ground state of $U^{4+}$ in the $Y_{1-x}U_xPd_3$ system [182–184], although the results are not consistent with one another. Mook et al. [182] inferred that the $U^{4+}$ groundstate is the $\Gamma_3$ non-magnetic doublet from INS measurements on $Y_{0.8}U_{0.2}Pd_3$, whereas Dai et al. [183] concluded that the $U^{4+}$ groundstate is the $\Gamma_5$ triplet from polarized INS studies of $Y_{1-x}U_xPd_3$ with $x=0.2$ and 0.45. Recently, Bull et al. [184] deduced that the $U^{4+}$ groundstate is the $\Gamma_3$ doublet with a low-lying $\Gamma_5$ triplet first excited state from INS measurements on $Y_{1-x}U_xPd_3$ with $x=0.2$, 0.28, 0.37 and 0.45. Furthermore, they observed that the low-energy excitation moves towards zero-energy transfer, with decreasing U concentration, leading to a groundstate in which the $\Gamma_3$ doublet and $\Gamma_5$ triplet states become nearly degenerate for $x=0.2$.

It should be noted that the U concentration range within which NFL behavior in the $Y_{1-x}U_xPd_3$ system is observed ($0<x\lesssim 0.2$) is contiguous with the region in which spin glass freezing occurs. This suggests that the NFL behavior in the physical properties at low temperature may be

associated with a magnetic quantum critical point (QCP) at $x \approx 0.2$. Andraka and Tsvelik [168], who performed measurements of $\rho$, $C$ and $M$ as a function of $T$ and $H$ on a $Y_{1-x}U_xPd_3$ specimen of composition $x = 0.2$, concluded from the scaling behavior of $C(T,H)$ and $M(T,H)$ with $H/T$, that the NFL behavior was associated with a second-order phase transition at $T = 0$ K.

### 7.2. The $U_{1-x}M_xPd_2Al_3$ (M = Y, Th) systems

During the last several years, we have identified two systems, $U_{1-x}M_xPd_2Al_3$ (M = Y, Th), that exhibit NFL behavior at low temperatures which apparently originates from two different mechanisms, an unconventional Kondo effect (M = Th) and fluctuations of an order parameter in the vicinity of an AFM quantum critical point (M = Y). Curiously, these two systems are derived by substituting different elements (Y and Th) into the same parent compound, $UPd_2Al_3$.

Temperature–composition ($T$–$x$) phase diagrams for the $U_{1-x}M_xPd_2Al_3$ (M = Y, Th) systems are shown in Fig. 24(a) and (b) for M = Th and Y, respectively [185]. The phase diagrams for the Th and Y substitutions are dramatically different. With increasing Th concentration $x$ below $x \approx 0.2$, $T_N$ and $T_c$ decrease only slightly [154,186], whereas the features in $\rho(T)$, $C(T)$ and $\chi(T)$ associated with the AFM and superconducting transitions are suppressed rapidly [154]. The small decrease of $T_N$ and $T_c$ with $x$ suggests that U is tetravalent in $U_{1-x}Th_xPd_2Al_3$ in the region where AFM order and SC are observed ($0 \leq x \lesssim 0.2$) [186].

As $x$ in the $U_{1-x}Th_xPd_2Al_3$ system is increased further, a crossover occurs in the range $0.2 \lesssim x \lesssim 0.4$ to a NFL regime for $0.6 \lesssim x \lesssim 1$. In the NFL regime, $\rho(T)$ and $\chi(T)$ exhibit Kondo-like behavior at high temperatures and NFL behavior at low temperatures $T < T_K$ [154,187]. The NFL characteristics in $\rho(T)$, $C(T)$ and $\chi(T)$ scale with U concentration $(1-x)$ and $T_K$, indicating that the NFL behavior is a single ion phenomenon, presumably associated with an unconventional magnetic moment screening mechanism (Kondo effect).

The U contributions to $\rho(T)$, $C(T)$ and $\chi(T)$ in $U_{1-x}Th_xPd_2Al_3$ have the following $T$ dependences: (i) $\Delta\rho(T) = \Delta\rho_c + \Delta\rho_K(T)$, where $\Delta\rho_K(T) = \Delta\rho_K(0)[1 - a(T/T_K)^n]$, with $n \approx 1.5$, $T_K \approx 20$ K, and $a \approx 0.2$ [188]. The potential scattering term $\Delta\rho_c$ and the Kondo scattering contribution $\Delta\rho_K(0)$ both scale with U concentration $(1-x)$ and the Kondo temperature $T_K$ is independent of $x$. (ii) $\Delta C(T)/T \propto -[(1-x)/T_K] \ln(T/T_K)$ [154,176] or $\Delta C(T)/T \propto (1-x)(T/T_K)^{-1+\lambda}$ with $\lambda = 0.8$ [189]. (iii) $\Delta\chi(T) \propto (1-x)(T/T_K)^{-1+\lambda}$ with $\lambda \approx 0.5$–$0.6$ [154,189]. Similar results for $\Delta\chi(T)$ were obtained by Strydom et al. [190].

The result that $T_K$ is independent of $x$ is consistent with tetravalency of U in $U_{1-x}Th_xPd_2Al_3$ in the NFL regime, similar to the tetravalency of U in the range $x \lesssim 0.2$ where AFM order and superconductivity are found, as inferred from the small changes of $T_N$ and $T_c$ with $x$. The $T^{3/2}$ behavior of $\Delta\rho_K(T)$ of $U_{1-x}Th_xPd_2Al_3$ is similar to that observed in the stoichiometric compounds $CePd_2Si_2$ and $CeIn_3$ at pressures near the critical pressure at which $T_N$ of these AFM compounds vanishes (and where superconductivity is observed) [157], and $CeNi_2Ge_2$ at atmospheric pressure [156]. Here, the $T^{3/2}$ behavior of $\Delta\rho(T)$ is attributed to AFM spin fluctuations in a three-dimensional (3-D) antiferromagnet with $T_N = 0$ K. However, in the $U_{1-x}Th_xPd_2Al_3$ system, there is no readily identifiable AFM QCP and the NFL behavior extends over a large range of Th composition $x$ and scales with $T_K$ and U composition $(1-x)$. Moreover, in the $U_{1-x}Y_xPd_2Al_3$ system, where there does appear to be an AFM QCP at $x_c \approx 0.7$, $\rho(T)$ is a linear function of $T$ at low temperatures for samples with $x$ near $x_c$, as described below.

In contrast to the $U_{1-x}Th_xPd_2Al_3$ system, $T_N$ and $T_c$ decrease rapidly to zero with increasing $x$ in the $U_{1-x}Y_xPd_2Al_3$ system, with NFL behavior occurring in the vicinity of the $x_c \approx 0.7$ QCP where $T_N$ vanishes [191]. In

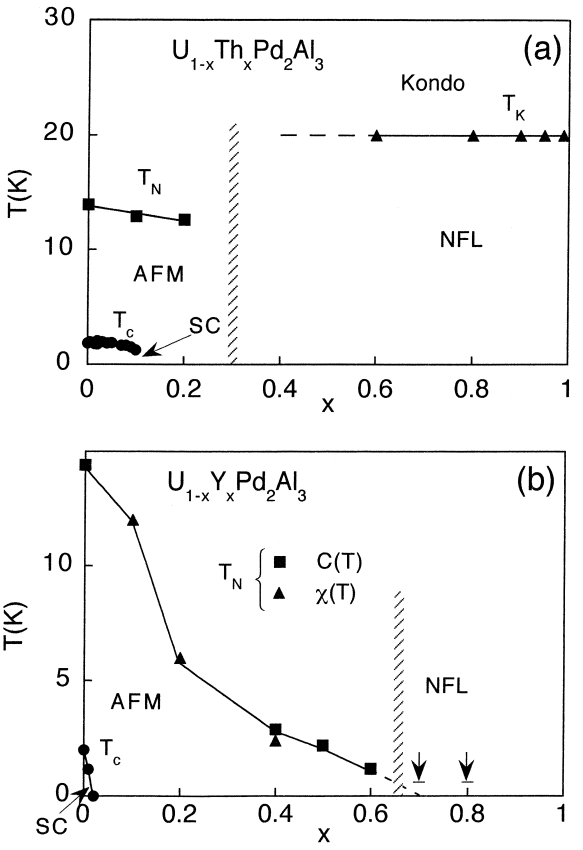


Fig. 24. Temperature–composition ($T$–$x$) phase diagrams for (a) $U_{1-x}Th_xPd_2Al_3$, and (b) $U_{1-x}Y_xPd_2Al_3$. Antiferromagnetic (AFM), superconducting (SC), Kondo, and non-Fermi liquid (NFL) regimes are identified in the figures. The meaning of the symbols are: $T_N$, Néel temperature; $T_K$, Kondo temperature; $T_c$, superconducting critical temperature. After Ref. [185].

the $U_{1-x}Y_xPd_2Al_3$ system, $\rho(T)$, $C(T)$ and $\chi(T)$ have the following $T$ dependences at low temperatures [191]: (i) $\rho(T) \propto T$ (0.1 K $\leq T \leq$ 7 K); (ii) $C(T)/T \propto -\ln T$ or $T^{-1+\lambda}$ with $\lambda \approx 0.8$ [191] (0.6 K $\leq T \leq$ 5 K); (iii) $\chi(T) \propto [1 - (T/T_o)^{1/2}]$ with $T_o \approx 30$ K (0.4 K $\leq T \leq$ 7 K). The NFL characteristics near the AFM QCP of the $U_{1-x}Y_xPd_2Al_3$ system are similar to those of the $CeCu_{6-x}Au_x$ system [192], where $T_N \propto (x - x_c)^{\mu}$ with $\mu \approx 1$, $\rho \propto T$, $C/T \propto -\ln T$, and $\chi \sim (1 - cT^{1/2})$. In the $CeCu_{6-x}Au_x$ system, this behavior has been suggested to be due to 2-D AFM spin fluctuations [193,194]. Further experiments will be required to determine whether a case can be made for 2-D spin fluctuations in the $U_{1-x}Y_xPd_2Al_3$ system, as well.

It is striking that substitutions of $Th^{4+}$ and $Y^{3+}$ lead to such dramatically different $T$–$x$ phase diagrams with NFL regimes that are apparently associated with different underlying mechanisms, single ion for $Th^{4+}$ and cooperative for $Y^{3+}$. Further research is needed to elucidate the NFL behavior and underlying mechanisms in the $U_{1-x}M_xPd_2Al_3$ (M = Y, Th) systems.

### *7.3. Pressure-induced superconductivity near magnetic quantum critical points*

Recently, Lonzarich et al. [157,195] reported measurements of the temperature dependence of the electrical resistivity of the AFM compounds $CeIn_3$ and $CePd_2Si_2$ at various pressures up to ~30 kbar. The Néel temperature $T_N$, determined from a discontinuity in the slope $d\rho/dT$ at $T_N$, was found to decrease slowly and monotonically with increasing $P$ for both compounds and to extrapolate to zero at a critical pressure $P_c$ of ~28 kbar for $CeIn_3$ and ~26 kbar for $CePd_2Si_2$. It was observed that near $P_c$, $\rho$ varies as $T^{1.6\pm0.2}$ for $CeIn_3$ and as $T^{1.2\pm0.1}$ for $CePd_2Si_2$ (over nearly two decades in temperature down to the milliKelvin range), indicative of NFL behavior for both compounds. For antiferromagnets near the QCP at $P_c$, $\rho(T)$ is expected to vary as $T^n$ with $n = 3/2$ in 3-D and 1 in 2-D, while $T_N$ is expected to vary as $(P - P_c)^{\mu}$ with $\mu = 2/3$ in 3-D and 1 in 2-D. The behavior of $\rho(T)$ and $T_N(P)$ near $P_c$ suggests that the spin fluctuations have 3-D character in cubic $CeIn_3$ and 2-D character in tetragonal $CePd_2Si_2$. At temperatures below 1 K and pressures in a narrow region near $P_c$, the resistivity was found to drop abruptly, indicative of superconductivity for both compounds. The AFM and superconducting regions in the $T$–$P$ phase diagram for $CePd_2Si_2$ are shown in Fig. 25. Displayed in the insets of Fig. 25 are the variation of $T_c$ with $P$ near $P_c$ (upper inset) and a plot of $\rho$ vs. $T^{1.2}$ at 28 kbar (lower inset). A similar $T$–$P$ phase diagram was found for $CeIn_3$. These observations suggest that the superconducting electron pairing is associated with AFM spin fluctuations, rather than phonons.

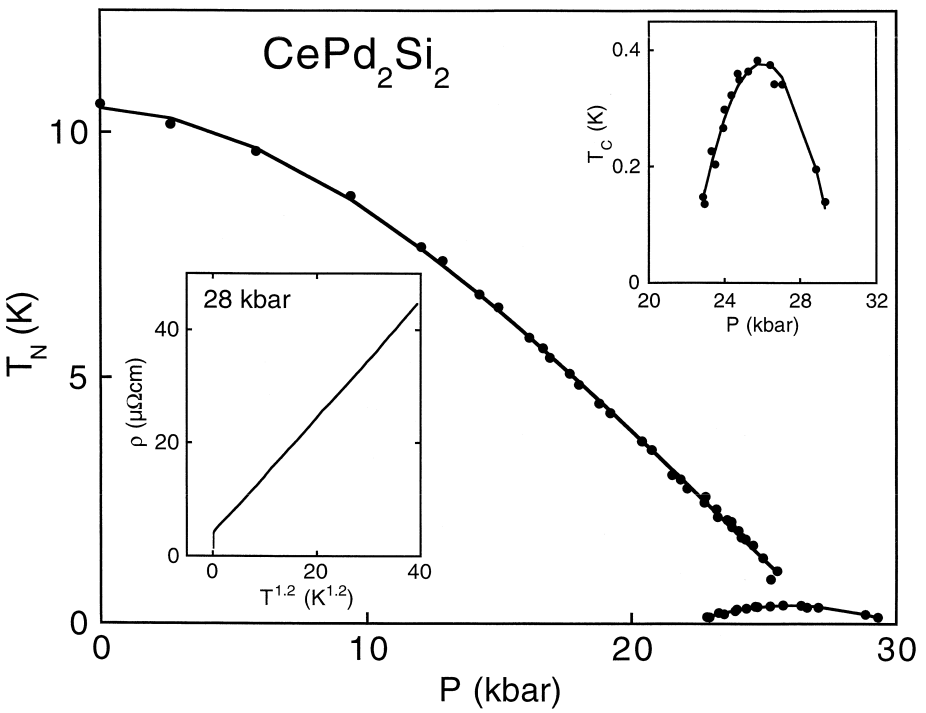


Fig. 25. Temperature–pressure ($T$–$P$) phase diagram of high-purity single-crystal $CePd_2Si_2$. Superconductivity occurs in a narrow range of pressure in the vicinity of the critical pressure $P_c$ where the Néel temperature $T_N$ tends to 0 K (antiferromagnetic quantum critical point). In the region near $P_c$, the $a$-axis resistivity in the normal state varies as $T^n$, where $n = 1.2 \pm 0.1$, over nearly two decades in temperature (lower inset). After Refs. [157,195].

## 8. Some remarks about high-temperature oxide superconductors

Part of the interest in non-Fermi liquid behavior in strongly correlated electron systems is associated with the unconventional superconductivity found in certain classes of these materials, such as the f-electron heavy fermion materials, considered herein, and the layered copper oxide high-$T_c$ superconductors, which have not been discussed in this article. A recent brief review of high-$T_c$ superconductivity in the cuprates by the author can be found in Ref. [196]. In spite of the disparity in the values of $T_c$, which are $\lesssim$2 K for the f-electron heavy fermion materials but as high as ~133 K for the layered copper oxide superconductors, the superconducting states of both of these materials share some striking similarities — the superconducting phase is in close proximity to an AFM phase along the composition or pressure axis, the superconductivity emerges from a non-Fermi liquid, the superconducting state appears to be anisotropic, with an energy gap that may vanish at points or lines on the Fermi surface, and the superconducting electron pairing may be mediated by AFM spin fluctuations. An understanding of the source of the NFL behavior in these systems may provide important information about the electronic structure and excitations in these systems, as well as the origin of the unconventional superconductivity. Based upon investigations of $La_{2-x}Sr_xCuO_4$, $YBa_2Cu_3O_{7-\delta}$, $YBa_2Cu_4O_8$, $Bi_2Sr_2CaCu_2O_8$, and other high-$T_c$ cuprate materials, one can construct a generic $T$–$x$ phase diagram which is shown schematically in Fig. 26. The phase diagram is very rich and contains insulating, AFM, superconducting, pseudogap, 2-D non-Fermi liquid-like, and 3-D Fermi liquid-like regions [196]. The similarity between the generic $T$–$x$ phase diagram for the high-$T_c$ cuprates shown in Fig. 26 and the f-electron compound $CePd_2Si_2$ displayed in Fig. 25 is certainly striking and suggests some common underlying physics for the two systems.

## 9. Epilogue

A brief survey of some of the remarkable electronic states and superconducting and magnetic phenomena that have been discovered in f-electron materials during the past three decades was presented in this paper. This survey was very selective, and the examples were largely drawn from the author's work. For comprehensive reviews of the subjects discussed herein, the reader is referred to various review articles cited throughout this paper.

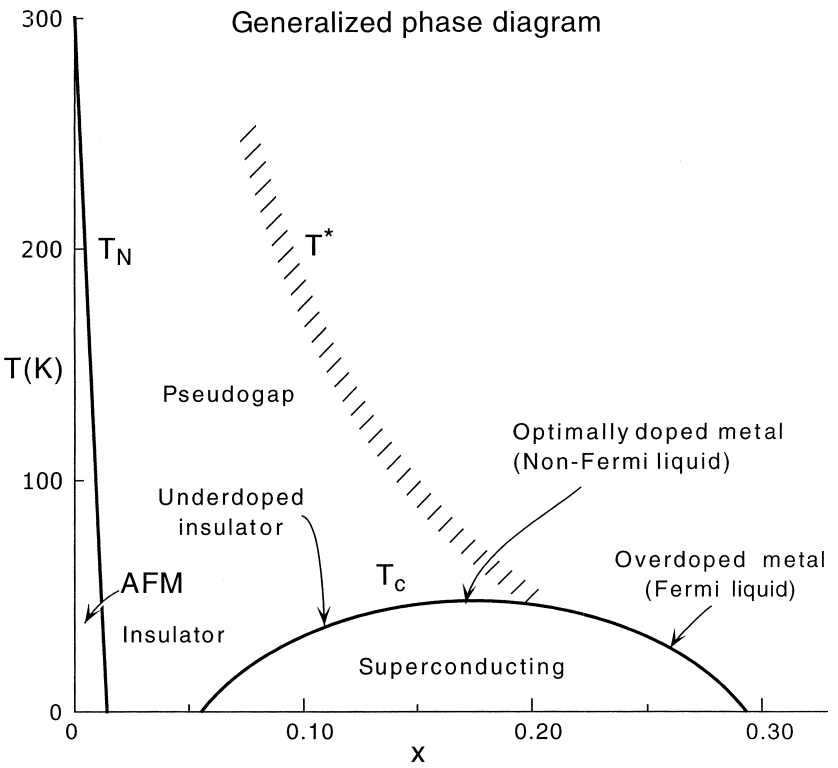


Fig. 26. Generic temperature–dopant concentration ($T$–$x$) phase diagram for cuprate superconductors (schematic). The solid lines labeled $T_N$ and $T_c$ delineate the antiferromagnetic (AFM) and superconducting regions, respectively. The 'hatched' line, denoted $T^*$, represents the crossover into the pseudogap state. After Ref. [196].

During my career, I have had the opportunity of working with many bright young graduate students and postdoctoral researchers on problems such as those described in this paper. I have also benefited from collaborations with numerous scientists throughout the world. In fact, the number of individuals with whom I have interacted is so large that I would not dare to list their names for the fear of leaving someone out. However, I would like to acknowledge two individuals who, unfortunately, left us before their time: The late Prof. Bernd T. Matthias, in whose laboratory I first became acquainted with the rare earths and from whom I learned, among other things, the excitement of research and discovery. The late Prof. Dieter K. Wohlleben, with whom I worked very closely on the subject of valence fluctuations in rare earth compounds, when we were both young graduate students and, later, postdoctoral research physicists in Matthias' laboratory. In the early years, Ben Ricks, a technician in the Matthias group, provided valuable technical support in the laboratory. No other person has had as important an impact on my work than my loyal assistant, Nancy McLaughlin, upon whose skill and wise counsel I have depended for many years. I would like to thank my wife, Margaret, and daughter, Elizabeth, for their support, encouragement, patience and understanding throughout my pursuits of research, such as that described herein. This work would not have been possible without the sponsorship of several federal research agencies. The Air Force Office of Scientific Research supported the research during the earlier years when I was a member of the Matthias group. I am especially grateful for the long-term research support provided by the US Department of Energy and the National Science Foundation. Eric Bauer and Robert Dickey kindly assisted in the preparation of this manuscript.

## References

[1] B.T. Matthias, H. Suhl, E. Corenzwit, Phys. Rev. Lett. 1 (1958) 92.
[2] C. Herring, Physica 24 (1958) S184.
[3] H. Suhl, B.T. Matthias, Phys. Rev. 114 (1959) 977.
[4] A.A. Abrikosov, L.P. Gor'kov, Zh. Eksp. Teor. Fiz. 39 (1960) 1781.
[5] A.A. Abrikosov, L.P. Gor'kov, Sov. Phys. JETP 12 (1961) 1243.
[6] P.G. deGennes, J. Phys. Radium 23 (1962) 510.
[7] M.B. Maple, Solid State Commun. 8 (1970) 1915.
[8] M.B. Maple, in: H. Suhl (Ed.), Magnetism: A Treatise on Modern Theory and Materials, Academic, New York, 1973, p. 289, Chapter 10.
[9] M.B. Maple, Phys. Lett. 26A (1968) 513.
[10] M.B. Maple, Solid State Commun. 12 (1973) 653.
[11] M.B. Maple, Z. Fisk, in: J.F. Allen, D.F. Finlayson, D.M. McCall (Eds.), Proc. 11th Intl. Conf. Low Temp. Phys., St. Andrews, Scotland, 1968, p. 1288.
[12] G. Riblet, K. Winzer, Solid State Commun. 9 (1971) 1663.
[13] M.B. Maple, W.A. Fertig, A.C. Mota, L.E. DeLong, D. Wohlleben, R. Fitzgerald, Solid State Commun. 11 (1972) 829.
[14] J.G. Huber, W.A. Fertig, M.B. Maple, Solid State Commun. 15 (1974) 453.
[15] S.D. Bader, N.E. Phillips, M.B. Maple, C.A. Luengo, Solid State Commun. 16 (1975) 126.
[16] P.E. Bloomfield, D.R. Hamann, Phys. Rev. 164 (1967) 856.
[17] A.B. Kaiser, J. Phys. C 3 (1970) 409.
[18] M.B. Maple, Appl. Phys. 9 (1976) 179.
[19] M.B. Maple, J.G. Huber, B.R. Coles, A.C. Lawson, J. Low Temp. Phys. 3 (1970) 137.
[20] J.G. Huber, M.B. Maple, J. Low Temp. Phys. 3 (1970) 537.
[21] J.G. Huber, M.B. Maple, Solid State Commun. 8 (1970) 1987.
[22] E. Müller-Hartmann, J. Zittartz, Phys. Rev. Lett. 26 (1971) 428.
[23] A. Ludwig, M.J. Zuckermann, J. Phys. F 1 (1971) 516.
[24] M.J. Zuckermann, Phys. Rev. 168 (1968) 390.
[25] E. Müller-Hartmann, J. Zittartz, Z. Phys. 234 (1970) 58.
[26] M.B. Maple, Z. Fisk, unpubl., 1968.
[27] M.B. Maple, Ph.D. Thesis, University of California, San Diego, 1969.
[28] H.J. van Daal, K.H.J. Buschow, Solid State Commun. 7 (1969) 217.
[29] K.H.J. Buschow, H.J. van Daal, Phys. Rev. Lett. 23 (1969) 408.
[30] K.H.J. Buschow, H.J. van Daal, Solid State Commun. 8 (1970) 363.
[31] P.F. Chester, G.O. Jones, Phil. Mag. 44 (1953) 1281.
[32] M.B. Maple, K.S. Kim, Phys. Rev. Lett. 23 (1969) 118.
[33] M.B. Maple, J. Wittig, K.S. Kim, Phys. Rev. Lett. 23 (1969) 1375.
[34] M.B. Maple, T.F. Smith, Solid State Commun. 7 (1969) 515.
[35] J.G. Huber, J. Brooks, D. Wohlleben, M.B. Maple, in: C.D. Graham Jr., G.H. Lander, J.J. Rhyne (Eds.), Magnetism and Magnetic Materials, No. 24, AIP Conf. Proc., 1975, p. 475.
[36] S. Ortega, M. Roth, C. Rizzuto, M.B. Maple, Solid State Commun. 13 (1973) 5.
[37] C.A. Luengo, J.G. Huber, M.B. Maple, M. Roth, Phys. Rev. Lett. 32 (1974) 54.
[38] C.A. Luengo, J.G. Huber, M.B. Maple, M. Roth, J. Low Temp. Phys. 21 (1975) 129.
[39] K.S. Kim, M.B. Maple, Phys. Rev. B 2 (1970) 4696.
[40] M.B. Maple, J. Wittig, Solid State Commun. 9 (1971) 1611.
[41] D.K. Wohlleben, M.B. Maple, Rev. Sci. Instr. 42 (1971) 1573.
[42] M.R. MacPherson, G.E. Everett, D. Wohlleben, M.B. Maple, Phys. Rev. Lett. 26 (1971) 20.
[43] M.B. Maple, D. Wohlleben, Phys. Rev. Lett. 27 (1971) 511.
[44] J.G. Huber, M.B. Maple, D. Wohlleben, G.S. Knapp, Solid State Commun. 16 (1975) 211.
[45] J.G. Huber, M.B. Maple, D. Wohlleben, J. Magn. Magn. Mat. 1 (1975) 58.
[46] K.A. Gschneidner Jr., R. Smoluchowski, J. Less-Common Met. 5 (1963) 374.
[47] E. Franceschi, G.L. Olcese, Phys. Rev. Lett. 22 (1969) 1299.
[48] A. Jayaraman, V. Narayanamurti, E. Bucher, R.G. Maines, Phys. Rev. Lett. 25 (1970) 1430.
[49] J.L. Kirk, K. Vedam, V. Narayanamurti, A. Jayaraman, E. Bucher, Phys. Rev. B 6 (1972) 3023.
[50] E. Bucher, V. Narayanamurti, A. Jayaraman, J. Appl. Phys. 42 (1971) 1741.
[51] A. Menth, E. Buehler, T.H. Geballe, Phys. Rev. Lett. 22 (1969) 295.
[52] J.C. Nickerson, R.M. White, K.N. Lee, R. Bachmann, T.H. Geballe, G.W. Hull Jr., Phys. Rev. B 3 (1971) 2030.
[53] M.B. Maple, D. Wohlleben, in: C.D. Graham Jr., J.J. Rhyne (Eds.), Magnetism and Magnetic Materials, No. 18, AIP Conf. Proc., 1974, p. 447.
[54] R.L. Cohen, M. Eibschütz, K.W. West, Phys. Rev. Lett. 24 (1970) 383.
[55] E.E. Vainshtein, S.M. Blokhin, Yu.B. Paderno, Sov. Phys. Solid State 6 (1965) 6318.
[56] J.M.D. Coey, S.K. Ghatak, M. Avignon, F. Holtzberg, Phys. Rev. B 14 (1976) 3744.
[57] M. Campagna, E. Bucher, G.K. Wertheim, L.D. Longinotti, Phys. Rev. Lett. 33 (1974) 165, for example.
[58] B.C. Sales, D.K. Wohlleben, Phys. Rev. Lett. 35 (1975) 1240.
[59] L.M. Falicov, W. Hanke, M.B. Maple (Eds.), Valence Fluctuations in Solids, North-Holland, Amsterdam, 1981, contains a review.

[60] M.S. Torkachvili, M.B. Maple, G.P. Meisner, in: U.U. Eckern, A. Schmid, W. Weber, W. Wühl (Eds.), Proc. LT–17, Elsevier, Amsterdam, 1984, p. 711.
[61] G.P. Meisner, M.S. Torikachvili, K.N. Yang, M.B. Maple, R.P. Guertin, J. Appl. Phys. 57 (1986) 3073.
[62] G. Aeppli, Z. Fisk, Comments Condens. Matter Phys. 16 (1992) 155.
[63] Ø. Fischer, A. Treyvaud, R. Chevrel, M. Sergent, Solid State Commun. 17 (1975) 721.
[64] R.N. Shelton, R.W. McCallum, H. Adrian, Phys. Lett. A 56 (1976) 213.
[65] B.T. Matthias, E. Corenzwit, J.M. Vandenberg, H. Barz, Proc. Natl. Acad. Sci. USA 74 (1977) 1334.
[66] Ø. Fischer, M.B. Maple (Eds.), Superconductivity in Ternary Compounds I, Topics in Current Physics, Vol. 32, Springer, Berlin, Heidelberg, New York, 1982, and references cited.
[67] M.B. Maple, Ø Fischer (Eds.), Superconductivity in Ternary Compounds II, Topics in Current Physics, Vol. 34, Springer, Berlin, Heidelberg, New York, 1982, and references cited.
[68] R.W. McCallum, D.C. Johnston, R.N. Shelton, M.B. Maple, Solid State Commun. 24 (1977) 391.
[69] H.C. Hamaker, L.D. Woolf, H.B. MacKay, Z. Fisk, M.B. Maple, Solid State Commun. 31 (1979) 139.
[70] M. Ishikawa, Ø. Fischer, Solid State Commun. 24 (1977) 747.
[71] M.B. Maple, L.D. Woolf, C.F. Majkrzak, G. Shirane, W. Thomlinson, D.E. Moncton, Phys. Lett. 77A (1980) 487.
[72] D.E. Moncton, G. Shirane, W. Thomlinson, M. Ishikawa, Ø. Fischer, Phys. Rev. Lett. 41 (1978) 1133.
[73] M.B. Maple, Physics Today 39 (1986) 72.
[74] P. Fulde, J. Keller, in: M.B. Maple, Ø. Fischer (Eds.), Superconductivity in Ternary Compounds II, Topics in Current Physics, Vol. 34, Springer, Berlin, Heidelberg, New York, 1982, Chapter 9, contains a review.
[75] H.C. Hamaker, L.D. Woolf, H.B. MacKay, Z. Fisk, M.B. Maple, Solid State Commun. 32 (1979) 289.
[76] M.B. Maple, H.C. Hamaker, L.D. Woolf, in: M.B. Maple, Ø. Fischer (Eds.), Superconductivity in Ternary Compounds II, Topics in Current Physics, Vol. 34, Springer, Berlin, Heidelberg, New York, 1982, Chapter 4.
[77] C.F. Majkrzak, S.K. Satija, G. Shirane, H.C. Hamaker, Z. Fisk, M.B. Maple, Phys. Rev. B 27 (1983) 2889.
[78] H.C. Hamaker, H.B. MacKay, M.S. Torikachvili, L.D. Woolf, M.B. Maple, W. Odoni, H.R. Ott, J. Low Temp. Phys. 44 (1981) 553.
[79] H. Eisaki, H. Takagi, R.J. Cava, B. Batlogg, J.J. Krajewski, W.F. Peck Jr., K. Mizuhashi, J.O. Lee, S. Uchida, Phys. Rev. B 50 (1994) 647.
[80] B.K. Cho, P.C. Canfield, D.C. Johnston, Phys. Rev. B 52 (1995) R3844.
[81] J.T. Markert, Y. Dalichaouch, M.B. Maple, in: D.M. Ginsberg (Ed.), Physical Properties of High Temperature Superconductors, I, World Scientific, Singapore, 1989, Chapter 6, contains a review.
[82] W.A. Fertig, D.C. Johnston, L.E. DeLong, R.W. McCallum, M.B. Maple, B.T. Matthias, Phys. Rev. Lett. 38 (1977) 387.
[83] M. Ishikawa, Ø. Fischer, Solid State Commun. 23 (1977) 37.
[84] M.B. Maple, H.C. Hamaker, L.D. Woolf, H.B. MacKay, Z. Fisk, W. Odoni, H.R. Ott, in: J.E. Crow, R.P. Guertin, T.W. Mihalisin (Eds.), Crystalline Electric Field and Structural Effects in f-Electron Systems, Plenum, New York, 1980, p. 533.
[85] H.R. Ott, W.A. Fertig, D.C. Johnston, M.B. Maple, B.T. Matthias, J. Low Temp. Phys. 33 (1978) 159.
[86] D.E. Moncton, D.B. McWhan, J. Eckert, G. Shirane, W. Thomlinson, Phys. Rev. Lett. 39 (1977) 1164.
[87] D.E. Moncton, D.B. McWhan, P.H. Schmidt, G. Shirane, W. Thomlinson, M.B. Maple, H.B. MacKay, L.D. Woolf, Z. Fisk, D.C. Johnston, Phys. Rev. Lett. 45 (1980) 2060.
[88] J.W. Lynn, D.E. Moncton, W. Thomlinson, G. Shirane, R.N. Shelton, Solid State Commun. 26 (1978) 493.
[89] S.K. Sinha, G.W. Crabtree, D.G. Hinks, H.A. Mook, Phys. Rev. Lett. 48 (1982) 950.
[90] J.W. Lynn, G. Shirane, W. Thomlinson, R.N. Shelton, D.E. Moncton, Phys. Rev. B 24 (1981) 3817.
[91] H.B. MacKay, M.B. Maple, unpubl., 1979.
[92] H.B. MacKay, Ph.D. Thesis, University of California, San Diego, 1979.
[93] M.B. Maple, in: E.C. Subbarao, W.E. Wallace (Eds.), Proc. Indo–US Conf. Science and Technology of Rare Earth Materials, Academic, New York, 1980, p. 167.
[94] P.W. Anderson, H. Suhl, Phys. Rev. 116 (1959) 898.
[95] E.I. Blount, C.M. Varma, Phys. Rev. Lett. 42 (1979) 1079.
[96] R.A. Ferrell, J.K. Bhattacharjee, A. Bagchi, Phys. Rev. Lett. 43 (1979) 154.
[97] H. Matsumoto, H. Umezawa, M. Tachiki, Solid State Commun. 31 (1979) 157.
[98] M. Tachiki, J. Magn. Magn. Mater. 31–34 (1983) 484.
[99] M.B. Maple, J. Magn. Magn. Mater. 31–34 (1983) 479.
[100] D.C. Johnston, W.A. Fertig, M.B. Maple, B.T. Matthias, Solid State Commun. 26 (1978) 141.
[101] H.A. Mook, O.A. Pringle, S. Kawarazaki, S.K. Sinha, G.W. Crabtree, D.G. Hinks, M.B. Maple, Z. Fisk, D.C. Johnston, L.D. Woolf, H.C. Hamaker, in: W. Buckel, W. Weber (Eds.), Superconductivity in d- and f-Band Metals, KFK, Karlsruhe, 1982, p. 201.
[102] L.D. Woolf, D.C. Johnston, H.A. Mook, W.C. Koehler, M.B. Maple, Z. Fisk, Physica 109 and 110B (1982) 2045.
[103] Z. Fisk, D.W. Hess, C.J. Pethick, D. Pines, J.L. Smith, J.D. Thompson, J.O. Willis, Science 239 (1988) 33.
[104] N. Grewe, F. Steglich, in: K.A. Gschneider Jr., L.L. Eyring (Eds.), Handbook of the Physics and Chemistry of the Rare Earths, Vol. 14, Elsevier, Amsterdam, 1991, p. 343.
[105] M.B. Maple, Physica B 215 (1995) 110.
[106] R.H. Heffner, M.R. Norman, Comments Condens. Matter Phys. 17 (1996) 361.
[107] S. Kondo, D.C. Johnston, C.A. Swenson, F. Borsa, A.V. Mahajan, L.L. Miller, T. Gu, A.I. Goldman, M.B. Maple, D.A. Gajewski, E.J. Freeman, N.R. Dilley, R.P. Dickey, J. Merrin, K. Kojima, G.M. Luke, Y.J. Uemura, O. Chmaissem, J.D. Jorgensen, Phys. Rev. Lett. 78 (1997) 3729.
[108] F. Steglich, J. Aarts, C.D. Bredl, W. Lieke, D. Meschede, W. Franz, H. Schafer, Phys. Rev. Lett. 43 (1979) 1892.
[109] H.R. Ott, H. Rudigier, Z. Fisk, J.L. Smith, Phys. Rev. Lett. 50 (1983) 1595.
[110] G.R. Stewart, Z. Fisk, J.O. Willis, J.L. Smith, Phys. Rev. Lett. 52 (1984) 679.
[111] W. Schlabitz, J. Baumann, B. Pollit, U. Rauchswalbe, H.M. Mayer, U. Ahlheim, C.D. Bredl, Z. Phys. B 62 (1986) 171.
[112] C. Geibel, S. Thies, D. Kaczorowski, A. Mehner, A. Grauel, B. Seidel, U. Ahlheim, R. Helfrich, K. Petersen, C.D. Bredl, F. Steglich, Z. Phys. B 83 (1991) 305.
[113] C. Geibel, C. Schank, S. Thies, H. Kitazawa, C.D. Bredl, A. Böhm, M. Rau, A. Grauel, R. Caspary, R. Helfrich, U. Ahlheim, G. Weber, F. Steglich, Z. Phys. B 84 (1991) 1.
[114] Y. Dalichaouch, M.C. de Andrade, M.B. Maple, Phys. Rev. B 46 (1992) 8671.
[115] A. Krimmel, P. Fischer, B. Roessli, H. Maletta, C. Geibel, C. Schank, A. Grauel, A. Loidl, F. Steglich, Z. Physik B 86 (1992) 161.
[116] Y. Kohori, K. Matsuda, T. Kohara, Solid State Commun. 95 (1995) 121.
[117] H. Tou, Y. Kitaoka, K. Asayama, C. Geibel, C. Schank, F. Steglich, J. Phys. Soc. Jpn. 64 (1995) 725.
[118] M. Jourdan, M. Huth, H. Adrian, Nature 398 (1999) 47.
[119] N. Bernhoeft, N. Sato, B. Roessli, N. Aso, A. Heiss, G.H. Lander, Y. Endoh, T. Komatsubara, Phys. Rev. Lett. 81 (1998) 4244.
[120] N. Metoki, Y. Haga, Y. Koike, Y. Onuki, Phys. Rev. Lett. 80 (1998) 5417.

[121] M.B. Maple, J.W. Chen, S.E. Lambert, Z. Fisk, J.L. Smith, H.R. Ott, J.S. Brooks, M.J. Naughton, Phys. Rev. Lett. 54 (1985) 477.
[122] J.L. Smith, Z. Fisk, J.O. Willis, A.L. Giorgi, R.B. Roof, H.R. Ott, H. Rudigier, E. Felder, Physica B 135 (1985) 3.
[123] H.R. Ott, H. Rudigier, Z. Fisk, J.L. Smith, Phys. Rev. B 3 (1985) 1651.
[124] R.H. Heffner, J.L. Smith, J.O. Willis, P. Birrer, C. Baines, F.N. Gygax, B. Hitti, E. Lippelt, H.R. Ott, A. Schenck, E. Knetsch, J.A. Mydosh, D.E. MacLaughlin, Phys. Rev. Lett. 65 (1990) 2816.
[125] S.E. Lambert, Y. Dalichaouch, M.B. Maple, J.L. Smith, Z. Fisk, Phys. Rev. Lett. 57 (1986) 1619.
[126] B.K. Sarma, M. Levy, S. Adenwalla, J.B. Ketterson, Phys. Acoustics XX (1992) 107.
[127] H.v. Löhneysen, Physica B 197 (1994) 551.
[128] J.A. Sauls, J. Low Temp. Phys. 95 (1994) 153, contains a review.
[129] R.A. Fisher, S. Kim, B.F. Woodfield, N.E. Phillips, L. Taillefer, K. Hasselbach, J. Flouquet, A.L. Giorgi, J.L. Smith, Phys. Rev. Lett. 62 (1989) 1411.
[130] K. Hasselbach, L. Taillefer, J. Flouquet, Phys. Rev. Lett. 63 (1989) 93.
[131] T. Trappman, H.v. Löhneysen, L. Taillefer, Phys. Rev. B 43 (1991) 13714.
[132] H.v. Löhneysen, T. Trappman, L. Taillefer, J. Magn. Magn. Mater. 108 (1992) 49.
[133] G. Goll, H.v. Löhneysen, I.K. Yanson, L. Taillefer, Phys. Rev. Lett. 70 (1993) 2008.
[134] G.M. Luke, A. Keren, L.P. Le, W.D. Wu, Y.J. Uemura, D.A. Bonn, L. Taillefer, J.D. Garrett, Physica B 186–188 (1993) 264.
[135] A. Amann, A.C. Mota, M.B. Maple, H.v. Löhneysen, Phys. Rev. B 57 (1998) 3640.
[136] B.S. Shivaram, Y.H. Jeong, T.F. Rosenbaum, D.J. Hinks, Phys. Rev. Lett. 56 (1986) 1078.
[137] Y. Dalichaouch, M.C. de Andrade, D.A. Gajewski, R. Chau, P. Visani, M.B. Maple, Phys. Rev. Lett. 75 (1995) 3938.
[138] Y. Kohori, T. Kohara, H. Shibai, Y. Oda, T. Kaneko, Y. Kitaoka, K. Asayama, J. Phys. Soc. Jpn. 56 (1987) 2263.
[139] Y. Kohori, H. Shibai, T. Kohara, Y. Oda, Y. Kitaoka, K. Asayama, J. Magn. Magn. Mater. 76–77 (1988) 478.
[140] G.M. Luke, L.P. Le, B.J. Sternlieb, W.D. Wu, Y.J. Uemura, J.H. Brewer, R. Kadono, R.F. Kiefl, S.R. Kreitzman, T.M. Riseman, Y. Dalichaouch, B.W. Lee, M.B. Maple, C.L. Seaman, P.E. Armstrong, R.W. Ellis, Z. Fisk, J.L. Smith, Phys. Lett. A 157 (1991) 173.
[141] H. Tou, Y. Kitaoka, K. Ishida, K. Asayama, N. Kimura, Y. Onuki, E. Yamamoto, Y. Haga, K. Maezawa, Phys. Rev. Lett. 80 (1998) 3129.
[142] M.B. Maple, J.W. Chen, Y. Dalichaouch, T. Kohara, C. Rossel, M.S. Torikachvili, M.W. McElfresh, J.D. Thompson, Phys. Rev. Lett. 56 (1986) 185.
[143] C. Broholm, J.K. Kjems, W.J.L. Buyers, P. Mathews, T.T.M. Palstra, A.A. Menovsky, J.A. Mydosh, Phys. Rev. Lett. 58 (1987) 1467.
[144] M.W. McElfresh, J.D. Thompson, J.O. Willis, M.B. Maple, T. Kohara, M.S. Torikachvili, Phys. Rev. B 35 (1987) 43.
[145] Y. Dalichaouch, M.B. Maple, J.W. Chen, T. Kohara, C. Rossel, M.S. Torikachvili, A.L. Giorgi, Phys. Rev. B 41 (1990) 1829.
[146] M.A. Lopez de la Torre, P. Visani, Y. Dalichaouch, B.W. Lee, M.B. Maple, Physica B 179 (1992) 208.
[147] A.P. Ramirez, B. Batlogg, E. Bucher, A.S. Cooper, Phys. Rev. Lett. 57 (1986) 1072.
[148] G.R. Stewart, A.L. Giorgi, J.O. Willis, J. O'Rourke, Phys. Rev. B 34 (1986) 4629.
[149] A. de Visser, J.C.P. Klaasse, M. van Sprang, J.J.M. Franse, A. Menovsky, T.T.M. Palstra, J. Magn. Magn. Mater. 54–57 (1986) 375.
[150] B. Batlogg, D.J. Bishop, E. Bucher, B. Golding, A.P. Ramirez, Z. Fisk, J.L. Smith, H.R. Ott, J. Magn. Magn. Mater. 63–64 (1987) 441.
[151] H. Amitsuka, T. Sakakibara, Y. Miyako, K. Sugiyama, A. Yamagishi, M. Date, J. Magn. Magn. Mater. 90–91 (1990) 47.
[152] Y. Dalichaouch, M.B. Maple, M.S. Torikachvili, A.L. Giorgi, Phys. Rev. B 39 (1989) 2423.
[153] P. Coleman, M.B. Maple, A.J. Millis (Eds.), Proc. Institute of Theoretical Physics Conf. on Non-Fermi Liquid Behavior in Metals, Santa Barbara, 1996; J. Phys.: Condens. Matter 8 (1996), see various articles.
[154] M.B. Maple, M.C. de Andrade, J. Herrmann, Y. Dalichaouch, D.A. Gajewski, C.L. Seaman, R. Chau, R. Movshovich, M.C. Aronson, R. Osborn, J. Low Temp. Phys. 99 (1995) 223.
[155] H.v. Löhneysen, J. Phys.: Condens. Matter 8 (1996) 9689.
[156] F. Steglich, B. Buschinger, P. Gegenwart, M. Lohmann, R. Helfrich, C. Langhammer, P. Hellmann, L. Donnevert, S. Thomas, A. Link, C. Geibel, M. Lang, G. Sparn, W. Assmus, J. Phys.: Condens. Matter 8 (1996) 9909.
[157] S.R. Julian, F.V. Carter, F.M. Grosche, R.K.W. Haselwimmer, S.J. Lister, N.D. Mathur, G.J. McMullan, C. Pfleiderer, S.S. Saxena, I.R. Walker, N.J.W. Wilson, G.G. Lonzarich, J. Mag. Mag. Mat. 177–181 (1998) 265.
[158] D.L. Cox, M.B. Maple, Physics Today 48 (1995) 32.
[159] P. Nozieres, A. Blandin, J. Phys. (Paris) 41 (1980) 193.
[160] A.M. Tsvelik, J. Phys. C 18 (1985) 159.
[161] D.L. Cox, Phys. Rev. Lett. 59 (1987) 1240.
[162] A.W.W. Ludwig, I. Affleck, Phys. Rev. Lett. 67 (1991) 3160.
[163] P. Schlottmann, P.D. Sacramento, Adv. Phys. 42 (1993) 641.
[164] O.O. Bernal, D.E. MacLaughlin, H.G. Lukefahr, B. Andraka, Phys. Rev. Lett. 75 (1995) 2023.
[165] E. Miranda, V. Dobrosavljevic, G. Kotliar, J. Phys.: Condens. Matter 8 (1996) 9871.
[166] T. Moriya, Spin Fluctuations in Itinerant Electron Magnetism, Springer, Berlin, 1985.
[167] T. Moriya, T. Takimoto, J. Phys. Soc. Jpn. 64 (1995) 960.
[168] B. Andraka, A.M. Tsvelik, Phys. Rev. Lett. 67 (1991) 2886.
[169] A.J. Millis, Phys. Rev. B 48 (1993) 7183.
[170] M.A. Continentino, Phys. Rev. B. 47 (1993) 11587.
[171] A.M. Tsvelik, M. Reizer, Phys. Rev. B 48 (1993) 9887.
[172] S. Sachdev, N. Read, R. Oppermann, Phys. Rev. B 52 (1995) 10286.
[173] A.H. Castro Neto, G. Castilla, B.A. Jones, Phys. Rev. Lett. 81 (1998) 3531.
[174] C.L. Seaman, M.B. Maple, B.W. Lee, S. Ghamaty, M.S. Torikachvili, J.-S. Kang, L.Z. Liu, J.W. Allen, D.L. Cox, Phys. Rev. Lett. 67 (1991) 2882.
[175] C.L. Seaman, M.B. Maple, B.W. Lee, S. Ghamaty, M.S. Torikachvili, J.-S. Kang, L.Z. Liu, J.W. Allen, D.L. Cox, J. Alloys Comp. 181 (1992) 327.
[176] M.B. Maple, R.P. Dickey, J. Herrmann, M.C. de Andrade, E.J. Freeman, D.A. Gajewski, R. Chau, J. Phys.: Condens. Matter. 8 (1996) 9773.
[177] M.B. Maple, C.L. Seaman, D.A. Gajewski, Y. Dalichaouch, V.B. Barbetta, M.C. de Andrade, H.A. Mook, H.G. Lukefahr, O.O. Bernal, D.E. MacLaughlin, J. Low Temp. Phys. 95 (1994) 225.
[178] C.L. Seaman, M.B. Maple, Physica B 199–200 (1994) 396.
[179] J.-S. Kang, J.W. Allen, M.B. Maple, M.S. Torikachvili, W.P. Ellis, B.B. Pate, Z.-X. Shen, J.J. Yeh, I. Lindau, Phys. Rev. B 39 (1989) 13529.
[180] P.D. Sacramento, P. Schlottmann, Phys. Lett. A 142 (1989) 245.
[181] D.L. Cox, M. Makivic, Physica B 199–200 (1994) 391.
[182] H.A. Mook, C.L. Seaman, M.B. Maple, M.A. López de la Torre, D.L. Cox, M. Makivic, Physica B 186–188 (1993) 341.
[183] P. Dai, H.A. Mook, C.L. Seaman, M.B. Maple, J.P. Koster, Phy. Rev. Lett. 75 (1995) 1202.
[184] M.J. Bull, K.A. McEwen, R.S. Eccleston, Phys. Rev. B 57 (1990) 3850.
[185] M.B. Maple, A. Amann, R.P. Dickey, E.J. Freeman, C. Sirvent, M.C. de Andrade, N.R. Dilley, Physica B, in press.

[186] C. Geibel, C. Schank, F. Jährling, B. Buschinger, A. Grauel, T. Lühmann, P. Gegenwart, R. Helfrich, P.H.P. Reinders, F. Steglich, Physica B 199–200 (1994) 128.
[187] Y. Dalichaouch, M.B. Maple, Physica B 199–200 (1994) 176.
[188] R.P. Dickey, A. Amann, E.J. Freeman, M.C. de Andrade, M.B. Maple, Phys. Rev. B, in press.
[189] M.C. de Andrade, R. Chau, R.P. Dickey, N.R. Dilley, E.J. Freeman, D.A. Gajewski, M.B. Maple, R. Movshovich, A.H. Castro Neto, G. Castilla, B.A. Jones, Phys. Rev. Lett. 81 (1998) 5620.
[190] A.M. Strydom, P. de V. du Plessis, R. Troc, Physica B 259–261 (1999) 421.
[191] E.J. Freeman, M.C. de Andrade, R.P. Dickey, N.R. Dilley, M.B. Maple, Phys. Rev. B 58 (1998) 16027.
[192] H.v. Löhneysen, T. Pietrus, G. Portisch, H.G. Schlager, A. Schröder, M. Siech, T. Trappmann, Phys. Rev. Lett. 72 (1994) 3262.
[193] A. Rosch, A. Schröder, O. Stockert, H.v. Löhneysen, Phys. Rev. Lett. 79 (1997) 159.
[194] O. Stockert, H.v. Löhneysen, A. Rosch, N. Pyka, M. Loewenhaupt, Phys. Rev. Lett. 80 (1998) 5627.
[195] N.D. Mathur, F.M. Grosche, S.R. Julian, I.R. Walker, D.M. Freye, R.K.W. Haselwimmer, G.G. Lonzarich, Nature 394 (1998) 39.
[196] M.B. Maple, J. Magn. Magn. Mater. 177 (1998) 18.